Performance comparison of artificial neural networks and expert systems applied to flow pattern identification in vertical ascendant gas–liquid flows

E.S. Rosa [a,*], R.M. Salgado [b], T. Ohishi [c], N. Mastelari [a]

[a] Mechanical Engineering Faculty, State University of Campinas, São Paulo, Brazil
[b] Exact Science Department, Federal University of Alfenas, Minas Gerais, Brazil
[c] Electrical and Computer Engineering Faculty, State University of Campinas, São Paulo, Brazil

ABSTRACT

Instantaneous readouts of an electrical resistivity probe are taken in an upward vertical air–water mixture. The signals are further processed to render the statistical moments and the probability density functions here used as objective flow pattern indicators. A series of 73 experimental runs have its flow pattern identified by visual inspection assisted by the analyses of the void fraction's trace and associated probability density function. The flow patterns are classified into six groups and labeled as: bubbly, spherical cap, slug, unstable slug, semi-annular and annular. This work compares and analyzes the performance of artificial neural networks, ANN, and expert systems to flow pattern identification. The employed ANNs are Multiple Layer Perceptrons, Radial Basis Functions and Probabilistic Neural Network, with single and multiple outputs. The performance is gauged by the percentage of right identifications based on experimental observation. The analysis is extended to clustering algorithms to assist the formation of knowledge base employed during the learning stages of the ANNs and expert systems. The performance of the following clustering algorithms: self organized maps, K-means and Fuzzy C-means are also tested against experimental data.

© 2010 Elsevier Ltd. All rights reserved.

1. Introduction

The flow of a gas–liquid mixture in a pipe is distinguished by the spatial distribution of the interfaces which separate the phases. In some flows the interfaces may evolve smoothly along the pipe while in other flows they assume complex shapes such as ripples, dendrites, dimples and irregular shapes that resemble fractals. The interfaces' shape and area density depend on the flow rates, fluid properties and pipe's size and orientation. By their turn, the interfaces with different shapes and area densities result in flows with distinct friction, heat and mass transfer coefficients. The coupling between the interface's shape and the interface's transport coefficients is one of the challenging aspects in two phase flow.

The development of transport equations to the interface's geometrical properties are not developed yet. In an attempt to overcome this deficiency a simpler approach is adopted by grouping the interfaces accordingly to their topological similarities and associating each group to a specific interfacial transfer mechanism to flow modeling. To classify the interfaces accordingly to their topological similarities were introduced the flow pattern or flow regime descriptors. They are based on written descriptions and on graphical illustrations which give a qualitative description of the phases'

spatial distribution. For example, a set of flow descriptors largely accepted in the literature for vertical gas–liquid flow is: the bubbly, the slug, the churn and the annular flow patterns as proposed by Taitel et al. (1980). The flow pattern identification results from the comparison of the visual observations against the qualitative descriptors. The method, based on the viewer's subjective criteria, lacks of a measurable quantity or objective parameter to pattern identification. In fact different viewers may arrive at distinct flow patterns identifications especially if the flow conditions lay on transition regions between neighboring patterns.

One of the first attempts to overcome the subjective criteria was proposed by Jones and Zuber (1975). Using X-rays, they measured the time-varying mean void fraction on the cross section of a 5 mm thick rectangular channel and plotted the probability density function, PDF, of these signals. Noticing the differences in the PDF's signatures for the distinct flow patterns the authors suggested it could be an objective flow pattern indicator. Alternatively, Tutu (1982) measuring the wall pressure fluctuation and the pressure drop of an upward air–water mixture flowing in a 52.2 mm ID also found the signal's statistical moments as objective flow pattern indicators.

These experimental techniques shaped two broad classes of methods for objective flow pattern indicators if one follows the criterion proposed by Drahos and Cermak (1989). One of the classes is based on the measurement of an energetic parameter: wall

* Corresponding author. Tel.: +55 019 3521 3268; fax: +55 019 3289 3722.
E-mail address: erosa@fem.unicamp.br (E.S. Rosa).

pressure fluctuation and wall shear stress fluctuation. The other class considers the measurement of some structural parameter with different responses to gas and liquid contents: gamma ray densitometer, electrical impedance method, optical method, ultra-sound and thermal anemometry among others. The development along these classes is still an active area nowadays. A brief survey based on the differential pressure measurements reports objective flow indicators arising from statistical moments of the differential pressure fluctuations (Matsui, 1984, 1986); fractal correlation dimension extracted from the fluctuating pressure signal (Cai et al., 1996); wavelet decomposition of the differential pressure signal (Elperin and Klochko, 2002) and the pressure's signal energy level decomposition using Hilbert–Huang transformation (Ding et al., 2007). Complementarily, a brief survey on the methods belonging to the second class shows objective flow indicators deriving from void fraction data. The signals are post-processed to extract: PDF, signal to noise ratio, spectral analyses and the Gabor's transform employing impedance probes sampling volumes or cross section areas (Wang et al., 1990; Costigan and Whalley, 1997; Song et al., 1998; Hervieu and Seleghim, 1998 and Lowe and Rezkallah, 1999); PDF from local resistivity probes (Das and Pattanayak, 1993); spatial–temporal distribution of echo intensities from ultra-sound pulses (Wada et al., 2006); PDF and wavelet analysis from parallel wire probe's signal (Jana et al., 2006) and Markov series of the local void fraction measured by optical probe (Mahvash and Ross, 2008).

The reviewed methods primarily transform a temporal signal into another quantity which more clearly expresses the distinctions among the flow patterns. Despite of the efforts none of these signal transformations perform satisfactory to flow pattern identification. In fact the signals are chaotic and governed by a high-order non-deterministic system. Therefore it is very likely that a single feature, extracted from the raw signal, will not be able to discriminate the flow patterns clearly. But, maybe, a combination of several of them will retain most of the data's original variability and render a better job as an objective indicator. The analysis of multiple input parameters faced a challenge on developing mapping procedures capable to relate multiple input data to the flow pattern labels. This difficulty was overcome during the 1990s with the application of Artificial Neural Networks, ANN, and classifiers algorithms to flow pattern identification problems.

The flow pattern identification techniques employing ANN are reviewed considering the applications with differential pressure transducers and electric impedance sensors as measuring devices. This choice is based on the increasing popularity of the association of ANNs with these measurement techniques in contrast to the use of Support Vector Machine (Tan et al., 2007) or else the use of image analysis of dynamic neutron radiographs videos (Tambouratzis and Pázsit, 2009). The advantages and disadvantages of the use of pressure transducers and impedance meters as measuring devices to flow pattern identification are briefed as follow. The pressure transducers have a low cost, are well developed, readily available to a large range of operational pressure and temperature, resistant to most of fluids and fulfill most of the operational safety regulations. The disadvantages are: the possibility of the pressure tap clogging, the lack of portability and the fact that the fluctuating pressure signal is not only dependent on the phases' distribution but also on the phases velocity. Here portability is defined as the capability of the ANN to be trained with a sensor or in a scaled down apparatus and to work similarly with distinct sensor or in actual size facilities. The impedance sensors have a raw output signal proportional to the void fraction. This feature, for being closely related to the flow pattern, demands less computational effort to map the signal features to the flow pattern. The disadvantages are that they are not commercially available neither are well developed for applications in new scenarios other than indoor controlled environments operating with mixtures of air–water or gas–oil.

The following review details the experimental apparatus including the line size and orientation, the measurement device, the data acquisition frequency and the sampling window, the objective flow pattern indicators and the mapping procedures. It starts with the applications of pressure fluctuating signal to flow pattern identification. Cai et al. (1994) sampled at 40 Hz the absolute pressure in a horizontal air–water pipe flow during 102.4 s to extract eight stochastic features. The features related to the amplitude domain were: standard deviation, skewness and kurtosis; the ones related to the frequency domain included: linear prediction coefficients and residual errors. The Kohonen self-organizing feature map, SOM, with eight input neurons was applied to cluster the input data into four groups corresponding to the slug, intermittent transition, wavy/stratified and bubbly flow patterns. Wu et al. (2001) took differential wall pressure measurements using piezoresistive transducers in a three-phase oil–gas–water flow. The test section is a horizontal pipe 40 mm ID and 206 pipe diameters long. The temporal pressure signal was denoised using wavelets and processed, using fractal theory, to give nine correlation dimensions. An ANN Multi-Layer Perceptron (MLP) having nine neurons for the input layer, five neurons for the hidden layer and a single neuron for the output layer was trained employing the back-propagation algorithm enhanced with a least square routine to render better stability and convergence speed. The network is trained to identify the stratified, intermittent and annular flow patterns. The reported misidentification rate is lower than 8%. Xie et al. (2003) trained an ANN-MLP to flow pattern identification in an upward vertical three phase flow of gas–liquid–pulp fiber mixture. They used as input data the wall pressure fluctuation signal sampled at 100 Hz to get the standard deviation, the skewness, the kurtosis plus seven other terms referring to auto-correlations at distinct time intervals. Two ANN's configurations with input, hidden and output layers having $10 \times 7 \times 4$ and $10 \times 7 \times 1$ were used for flow pattern identification. Both ANN-MLP were capable of identify the bubbly, plug, churn and slug flow pattern with a misidentification rate of 7%. Xie et al. (2004) extended the analysis using the normalized pressure power spectral density, PSD, instead of the auto-correlations of the pressure signal. An ANN-MLP with $8 \times 5 \times 1$ neurons corresponding to the input, hidden and output layers, was trained with a six level decomposition of the PSD showing a good discrimination among the flow patterns. The authors claim that the arrangement of the ANN with the PSD gives a better portability to the identification system as compared with the previous work Xie et al. (2003).

The survey is completed with the applications of ANN to flow pattern identification employing electrical impedance probes as measuring devices. Mi et al. (1998) employed ANN-MLP and ANN-SOM to flow pattern identification. A total of 28 runs were performed in a vertical 50.8 mm ID pipe with air and de-ionized water. The impedance sensor was installed 60D from the inlet. It consisted of eight circular electrodes with 9.5 mm diameter uniformly spaced along the pipe perimeter flush mounted in a 50.8 mm inside diameter pipe. The signals were sampled at 200 Hz during 60 s. The ANN-MLP had four input nodes corresponding to the mean and standard deviation of the diagonal and neighboring electrodes. The output layer has a single neuron to identify four patterns: bubbly, slug, churn and annular. The ANN-SOM has the same input layer employed by the ANN-MLP but its output layer has two configurations with four or seven output neurons corresponding, respectively, to the already listed flow patterns or including the transitions between each pattern. Both types of ANNs with four output nodes show an identification rate of 96%. The disagreement occurs at points laying on the transition boundary between slug and churn flow and also between churn

and annular flow. The ANN-SOM with seven output nodes was able to resolve the transition boundaries and has an identification rate of 100% out of 28 samples. Yan et al. (2004) extend the concept developed by Mi et al. (1998) to an electrical capacitance tomography aimed to objectively identify gas–liquid flow patterns. It is a theoretical work in a sense that they numerically simulated the signals from eight electrodes flush mounted along the pipe rim through a 2D finite element code. The steady state values of the eight electrodes are combined in arrangements involving the diagonal, adjacent and second adjacent electrodes and expressed by the mean and standard deviations of the sums of the electrodes. An ANN-MLP with $10 \times 10 \times 8$ neurons corresponding to the input, hidden and output layers, respectively, was trained to flow pattern identification in gas–liquid horizontal flows. The mismatch rate is of 6.3%. The method is promising but it lacks from experimental evidence since the actual signals are not steady and the edge effects existing on finite electrodes are not captured by the 2D numerical simulations. Hernandez et al. (2006) employed a double wire needle-contact probe, placed at the pipe center-line, to detect the bubbles' cord length in an upward air–water flow. The tests were in a 50.8 mm ID pipe with the probe placed 67D downstream of the air–water mixer. The sensor's signal is sampled at 12KHz, acquired, denoised, normalized, applied to a threshold value technique and processed to get the interface velocity and the bubble's cord length. A total of 125 tests were conducted to capture the features of five flow patterns: bubbly, cap-bubbly, slug, churn-turbulent and annular. The resultant cumulative probability functions of the bubbles' cords length were selected as input parameters. Two types of ANNs were used: the PNN and the SOM together with two data compressing techniques and different training strategies. The optimized configuration was the ANN-PNN with 95% of positive identification. Some specific classification problems were concentrated along the transition between churn-turbulent and annular flow patterns. Juliá et al. (2008) advance the work of Hernandez et al. (2006) by measuring the bubbles' cord length at three radial positions simultaneously, getting the cumulative probability function and adding the three cord length distributions to extract global flow information instead of a local information. Juliá employs the same experimental apparatus described in Hernandez et al. (2006). The signals were sampled during 1960s and self-clustered employing the SOM algorithm. The ANN-SOMs sensitivity is explored by clustering data into 3, 4 or 5 categories which, after processing, are labeled according to the flow pattern labels already listed in Hernandez et al. (2006). When the data were clustered into five categories the SOMs algorithm failed to distinguish between churn and annular patterns. Finally, Lee et al. (2008) compare the performance of a supervised ANN-MLP and a non-supervised ANN-SOM in vertical air–water flows using an impedance meter with multiple electrodes, as described by Mi et al. (1998). The test section consists of two vertical pipes with ID of 2.54 cm and 5.08 cm and total lengths of 150D and 75D, respectively. The impedance probes were placed at 34D and 63D from the entrance for test sections with 2.54 cm and

5.08 cm ID pipes, respectively. The sampling frequency and the data acquisition period were, respectively, of 100 Hz and 1 s. The short acquisition period is to allow flow pattern identification in transient regimes. The raw signal is normalized and sorted, accordingly to its magnitude, to form a sequence of crescent values resembling a cumulative distribution function. The ordered sequence of values is used as input to the ANNs. Both ANNs have 100 input nodes. The architecture of the ANN-MLP has seven hidden nodes and five output nodes corresponding to the bubbly, spherical cap, slug, churn-turbulent and annular flow patterns. An ANN-SOM is used to cluster the cumulative distribution functions and, in a post work stage, was attributed to each cluster a corresponding flow pattern label. The representativeness of the clustered data in regard to the flow pattern was gauged by ordering the data into 3, 4 and 5 groups. The ANN-SOM failed to recognize the churn-turbulent and annular patterns in any of these configurations; as a matter of fact it always grouped them into the same single cluster. Nevertheless the outputs of the ANN-MLP agreed with the Mishima and Ishii (1984) transition criteria for upward gas–liquid flow in vertical pipes.

The reviewed flow pattern identification methods can be summarized into three operational blocks: (i) measuring device, (ii) signal processing, and (iii) flow pattern identification technique, see Fig. 1. The measuring device block involves the experimental apparatus and the transducer type to extract a temporal signal dependent on the flow pattern. The data processing block has as input/output a temporal series and an objective flow pattern indicator, respectively. The input signal may be submitted to a large variety of transformations to get objective flow pattern indicators. The flow pattern identification block maps the flow pattern indicators to a given flow pattern label employing non-linear mapping techniques with multiple input parameters based on ANN.

The reviewed applications of ANN to flow pattern identification were successfully accomplished with positive identification rate higher than 90%. But the diversity of procedures regarding the measuring device, experimental apparatus, pipe orientation, signal processing and ANN architectures avoids a direct comparison among the works. For example, one may consider as a measuring device the fluctuating pressure or the impedance meters including, single and multiple electrodes for global or local measurement which in turn may be non-intrusive or intrusive. Moreover, the signals acquisition frequency and period spanned from 40 Hz to 12 KHz and from 1 s to 100 s, respectively. Also for objective flow pattern indicator were found as statistical moments, power spectral densities, wavelet decompositions, Hilbert–Huang transform, PDF, among other types of signal processing. Finally, the employed ANNs are based on a learning stage such as ANN-MLP, ANN-RBF and ANN-PNN but also on clustering algorithms such as ANN-SOM.

Beyond the diversity of procedures quoted above, most of the works does not employ the same flow pattern labels which, in some circumstances, makes unease to establish a comparison. For example some authors simply adopt intermittent flows while others employ elongated bubble and slug. The non-similarities also
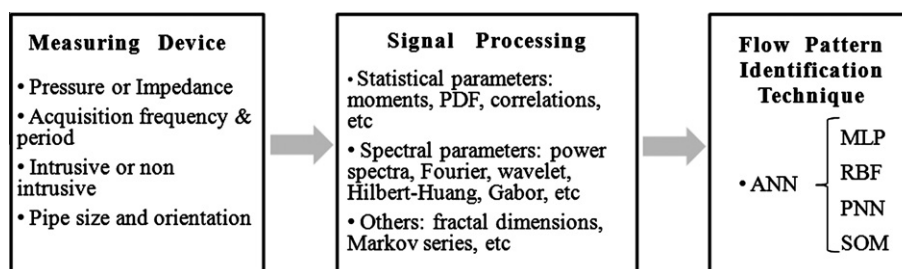

Fig. 1. Flow pattern identification block diagram.

arise due to the number of flow patterns, some authors prefer to employ four groups: bubbly, slug, churn and annular while others include the transitional patterns adding, at least, two or three more groups. A fair comparison among the techniques exists if all of them worked with the same number of flow patterns labels. At last, some works, due to experimental constraints, test the identification techniques over a limited area of the flow map not covering all possible flow patterns or, with a few number of data samples in certain flow patterns which may compromise the learning stage of these techniques.

1.1. Objective

This work main's objective is to draw comparisons among different techniques employing the same data base. Specifically, it develops a performance's analysis of: (i) clustering algorithms; (ii) mapping techniques and iii) the influence of the input data.

The text organization follows the block structure depicted in Fig. 1. The description of the experimental apparatus and the introduction of a novel resistivity probe are in Section 2. The instantaneous line averaged void fraction is processed to render the first four statistical moments and its PDF. The data processing and the flow pattern labeling criteria are in Section 3. Section 4 presents the flow pattern identification techniques, Section 5 shows the results and, finally, the conclusions are in Section 6.

2. Experimental apparatus and measuring device

The flow patterns of an upward co-current air–water mixture were reproduced experimentally in a facility shown schematically in Fig. 2. A reciprocating compressor and a centrifugal pump supply air and water to the mixer installed at the entrance of the vertical test section with 26 mm ID and 306D long. At the exit of the test section there is a long radius U bend which directs the mixture to a drop leg 75 mm ID. The air and the water are primarily separated at the drop leg. The air is freely discharged into the atmosphere by the annular gap between the pipes. The water flows downward to a collecting tank which, being 1.5 m in diameter, has a large enough residence time to separate the small air bubbles eventually carried by the downstream water flow. The water exits the tank to feed the centrifugal pump in a closed loop. The tests were conducted at nearly atmospheric pressure of 946 mBar and ambient temperature of 24 °C ensured by the system water total volume of 3 m^3. Two Merian laminar flow elements with reported uncertainty of 2% are used to measure the air flow rate within the range of 0–0.21 Sm^3/min and 0–0.65 Sm^3/min. The water flow rate measurement uses two flow meters: a Metroval Coriolis and a Fisher Vortex both calibrated at 1½% of uncertainty operating within the range of 12–55 kg/min and 26–200 kg/min, respectively. The air and the water flow rates as well as the temperature and pressure were continuously monitored, controlled and registered by the supervisory system.

2.1. The measuring device

The measuring device is a single-wire resistivity probe placed at 257D downstream of the air–water mixer followed by a straight transparent Plexiglas pipe to aid the flow pattern visualization. The probe consists of a bare stainless steel cylindrical rod with 0.6 mm in diameter stretched along the pipe diameter line resulting in an area blockage ratio less than 3%. A metallic pipe houses the cylindrical rod. Sleeves placed at the pipe rim fix the rod at the pipe providing to the rod mechanical support, electrical insulation and a seal avoiding water or air leakages, see schematic in Fig. 3a.
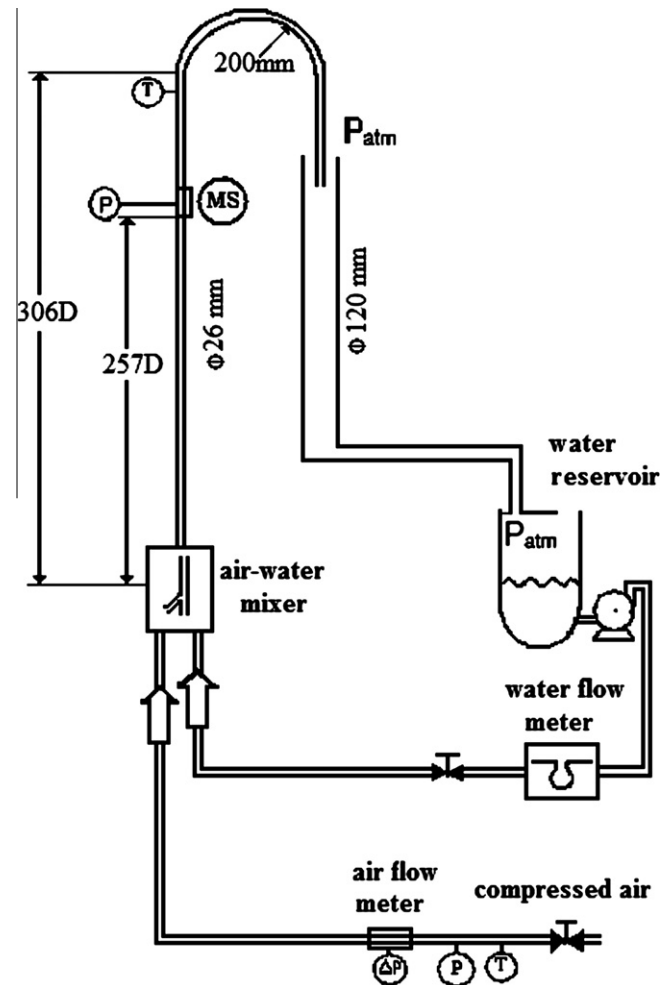
Fig. 2. Schematic representation of the experimental apparatus.

The probe's signal is proportional to the electrical resistance of the water path established between the wetted area of the rod and the pipe wall. Furthermore, the rod to pipe diameter ratio of 0.023 constrains the probe's sensitivity into a small volume concentric to the rod axis. The sensing volume is approximately described by a radial distance of nearly two rod diameters with an axial extension equivalent to the wetted portion of the rod. It is suited to measure water layer heights in stratified flows, Fig. 3b, but also the equivalent water layer height, EWLH, in dispersed bubbly flows due its small sensitivity along rod's the radial direction. The EWLH corresponds to the rod's wetted axial extension; see Fig. 3c. Additionally, the ratio of the EWLH to the pipe diameter is interpreted as the line averaged liquid hold-up. The probe's operational principle bears similarity to the single-wire capacitive probe described in Huang et al. (2008).

The probe's circuit is a voltage divider driven by an oscillator as depicted in Fig. 4. The oscillator's output is a 100 kHz sinusoidal signal with 10 V rms to minimize the polarization effects on the probe contact surface. The probe's resistance is a variable resistance represented by R_p; R_p is a constant resistance and the voltage drop on the probe is V_m. The probe resistance is proportional to the water resistivity, ρ, and inversely proportional the EWLH, or simply ℓ:

$$R_p = \rho C/\ell, \tag{1}$$

where C is a dimensionless shape factor due to the rod to pipe geometry. When the tube is full of water R_p takes its lowest value:
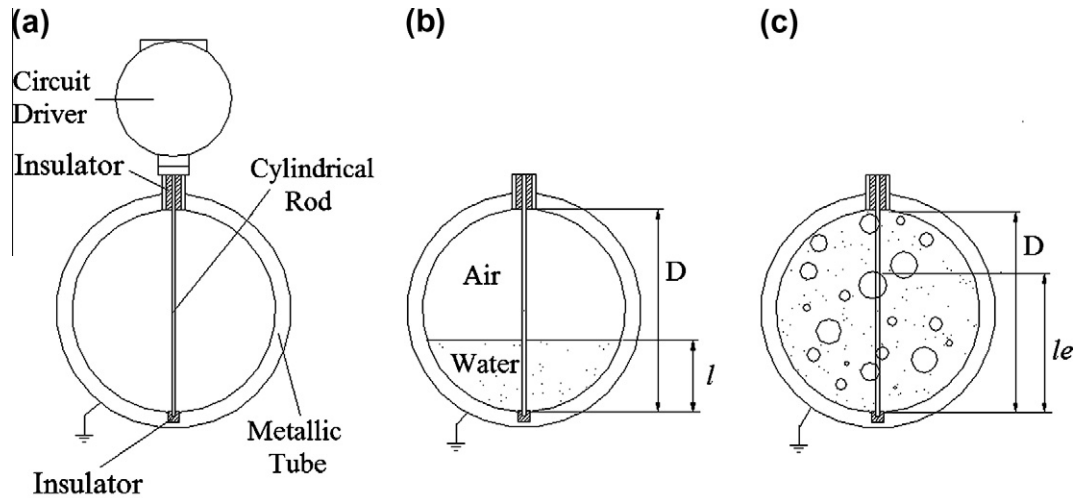
Fig. 3. Probe elements (a), representation of the water layer height for stratified flow (b) and the equivalent water layer height for dispersed flow (c).
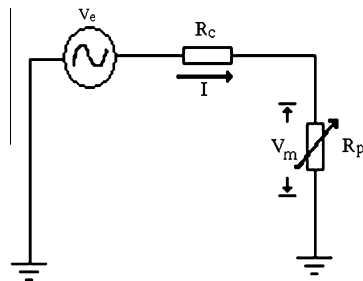
Fig. 4. Schematic representation of the probe's driving circuit.

$$R_p^L = \rho C/D, \tag{2}$$

where D is the pipe diameter. Conversely, when the tube is full of air, $\ell = 0$, R_p takes its highest value, $R_p \equiv R_p^H \to \infty$. The voltage drop on the probe is determined by:

$$V_m = \frac{V_e}{\left(1 + \frac{R_c}{R_p}\right)}. \tag{3}$$

The line averaged void fraction is defined a function of the voltage ratio:

$$\varepsilon = f\left(\frac{V_m - V_L}{V_H - V_L}\right). \tag{4}$$

The values for V_H and V_L are determined by substituting the definitions of R_p^H and R_p^L into Eq. (3). The function f is unknown but ε and the voltage ratio span from 0 to 1. Furthermore, at the extremes, $V_m = V_L$ or $V_m = V_H$, the argument of f and ε are coincident, i.e., $f(0) = 0$ and $f(1) = 1$. Forcing, by design criterion, the ratio $R_c/R_p^L \leqslant \frac{1}{20}$; then it is possible to express the voltage ratio as function of the probe resistances' ratio which, by its turn is coincident with the complement of the EWLH or to the line averaged void fraction itself

$$\left(\frac{V_m - V_L}{V_H - V_L}\right) \cong \left(1 - \frac{R_p^L}{R_p}\right) \equiv \left(1 - \frac{\ell}{D}\right) \equiv \varepsilon. \tag{5}$$

3. Signal acquisition, processing and labeling

This section presents: the raw signal, the post processing technique, the flow pattern descriptors, and the definitions of the training and test data sets.

3.1. Raw signal acquisition

The voltage drop on the probe, V_m, is sampled at a 3 kHz for a period of 60 s for each run using a National Instruments acquisition board SCXI-1308. The sampling frequency is 10–20 times higher than the highest frequency component of the signal assuring all signals information is preserved. Certainly it is possible to work with a lower sampling rate but a study of the optimum sampling frequency is considered out of the scope of this work. The sampling period is of 60 s. This value guarantees representative data samples for all analyzed flow patterns and, in particular, to the intermittent flow patterns which present the lowest frequencies, typically from 1 Hz up to 10 Hz in this experimental facility. The 60 s period assures data samples with at least 60 liquid pistons followed by elongated gas bubbles. A short analysis employing double and triple acquisition periods for slug flow pattern disclose changes on the first four statistical moments less than 1%. The data is post-processed to compensate eventual changes on the water resistivity due to temperature or ion concentration changes during the tests. For reference the trace of the instantaneous line averaged void fraction, ε, typical of each flow pattern are displayed in Fig. 5.

3.2. Signal processing technique

The trace of the line averaged void fraction is processed to render the signal's first four statistical moments as well as the signals PDF, see Fig. 5. The choice of the statistical moments or the PDF in place of other type of signal's transformation is because they are physically attached to the shape of the void fraction distribution which, by its turn, is closely related to the flow pattern, Jones and Zuber (1975).

The spanning interval of the line averaged void fraction, $0 \leqslant \varepsilon \leqslant 1$, is divided into 300 bins. The discrete occurrences of ε in each bin are smoothed (Bowman and Azzalini, 1997) to get an estimate of the PDF. The use of a PDF instead of a histogram proved to be more efficient to the flow pattern identification because the smoothing technique allows a PDF with stable shape while the histogram's shape is sensitive to the number of bins.

3.3. Experimental data classification criteria and flow pattern descriptors

A human specialist identified the flow patterns by combining visual information, either by naked eye or aided by digital high
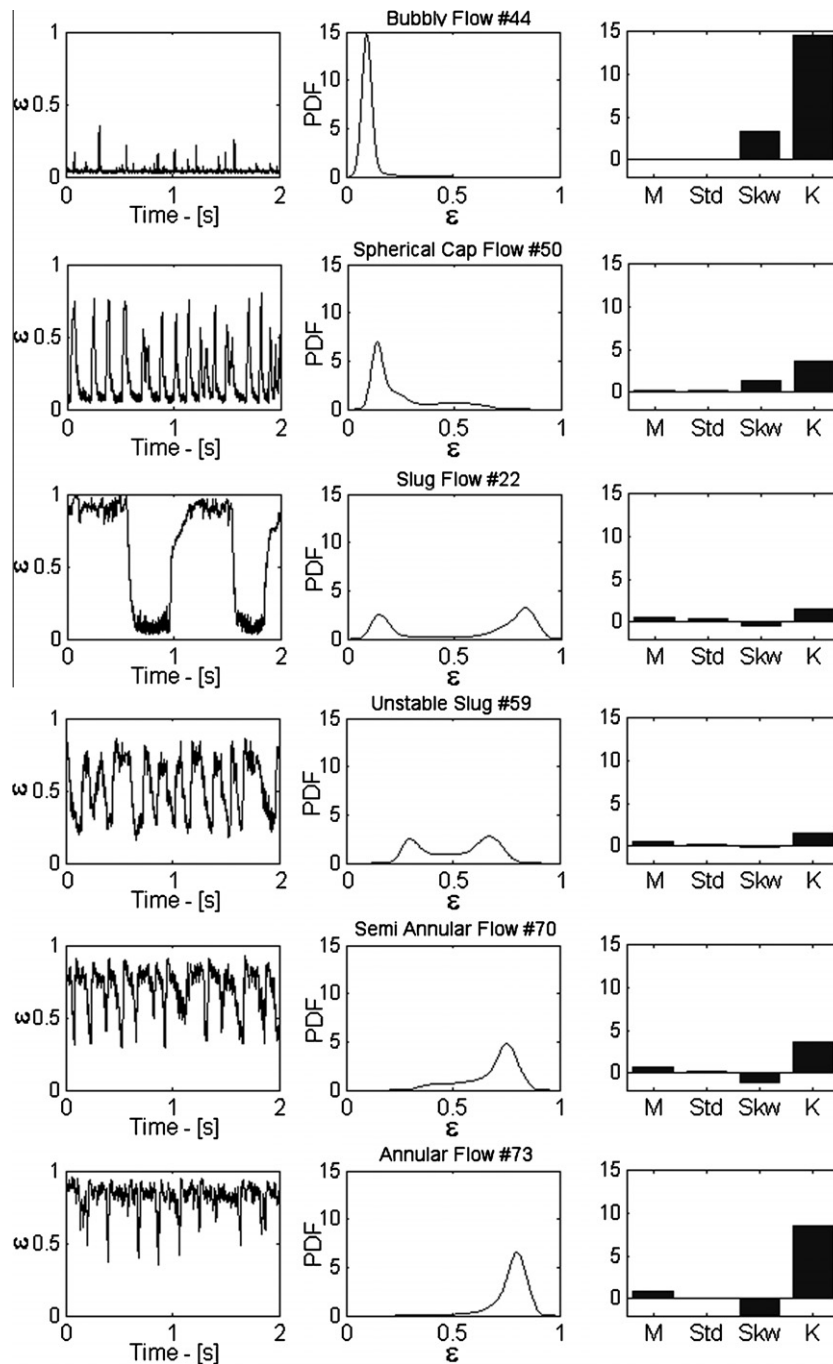
Fig. 5. Typical line averaged void fraction traces, PDFs, and statistical moments. M, Std, Skw and K stand for mean, standard deviation, skewness and kurtosis of the line averaged void fraction.

speed photographs, with the analysis of the instantaneous line averaged void fraction and its PDF. The second approach complements the visual observations since the instantaneous readings of ε gives information on how ε changes with time while its PDF discloses the most observed values during the time series. Similar approaches have been used by Costigan and Whalley (1997), Song et al. (1998), and Omebere-Iyari et al. (2008), for example.

The flow patterns are classified into six groups: bubbly flow, spherical cap flow, slug flow, unstable slug flow, semi-annular flow and annular flow instead of the established four groups: bubbly, slug, churn and annular flow patterns. A visual identification of each flow pattern is on Fig. 6. The choice of six instead of four groups is to capture, more clearly, the transitions regions between

adjacent flow patterns. Furthermore, the usage of churn as flow descriptor is replaced by the unstable slug flow and semi-annular flow to avoid ambiguity often associated with it, see for example Jayanti and Hewitt (1992), Hewiit and Jayanti (1993) and Costigan and Whalley (1997).

The flow patterns descriptors are as follows.

The Bubbly flow encompasses the representation of mono-dispersed bubbles as well as bubble clusters also known by discrete bubbles. The first sub-pattern applies to bubbles with uniform sizes describing rectilinear trajectories with no interaction between neighboring bubbles. The clustered bubbles represent bubbles with a non-uniform size and non-spherical shapes describing a zig-zag trajectory. The trace of ε ranges oscillates within
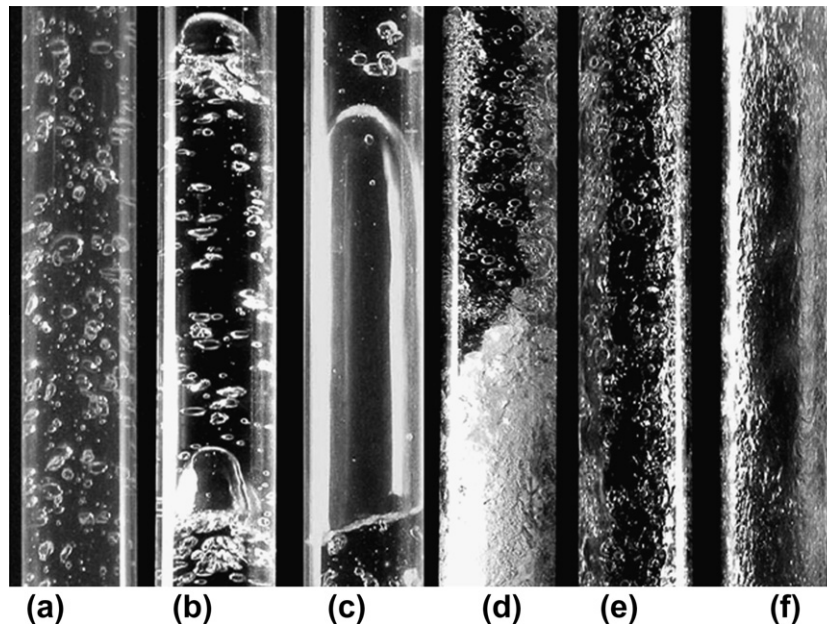
Fig. 6. Test section photographs of upward air–water flow exhibiting the visual flow patterns features: (a) bubbly; (b) spherical cap; (c) slug; (d) unstable slug; (e) semi-annular and (f) annular.

0.025 up to 0.4 with a mean value always lower than 0.1. The correspondent PDF has a sharp peak, with positive or null skew depending if there are bubble clusters or not. For reference Fig. 5 exhibits a time record window of 2 s and the associated PDF corresponding to discrete bubbles flow pattern. Although, not observed during the experimental tests, there is also a third classification for the bubbly flow pattern: the churn-turbulent bubbly flow. It consists of highly agitated distorted bubble clusters with several pipe diameters of axial length characterized by single peaked PDF with null or positive skew. This flow pattern is found on large diameter pipes, see Omebere-Iyari et al. (2008), but also is related to the entrance phenomena occurring near the pipe inlets.

The Spherical Cap flow is characterized by bubbles which may take partially the pipe cross section in a capped void, as originally described in Davies and Taylor (1950). Once the cap bubbles are formed, the trailing cap catches up and coalesces with the leading cap ultimately leading to a short Taylor bubble. The trace of ε has large oscillations between 0.1 and 0.8 with typical mean value within 0.1 and 0.2. The PDF has a small peak if compared with the bubbly flow and a large positive skew. A typical trace and PDF of the spherical cap flow is shown in Fig. 5. Usually the spherical cap flow is grouped with the clustered bubbly flow, Taitel et al. (1980).

The Slug flow is viewed as the succession of aerated liquid pistons followed by an elongated bullet shaped gas bubbles, often called by Taylor bubbles, flowing up surrounded by a liquid film. The persistence of the signal at low or high values of ε corresponds to the transit of a liquid slug or a gas bubble by the sensor. The intermittent flow nature is clearly distinguished by the trace because the signal is either low or high with stepwise transition between states. The PDF has two peaks in correspondence with the gas and liquid occurrences. As an example Fig. 5 brings the trace and PDF of a typical slug flow signature. As a final remark, slug flow is also called by plug flow although, for horizontal flows, some authors make distinctions between plug and slug accordingly to the bubble's tail shape (Ruder and Hanratty, 1990; Fagundes Netto et al., 1999).

The Unstable Slug flow was designated after Costigan and Whalley (1997) as a flow pattern succeeding the slug flow when the gas flow rate increases. This designation is not unique; usually it is referred as churn flow, churn-turbulent flow or also as froth flow. But, these flow patterns have broader signification in a sense that they mean not only the slug transition when the gas flow rate increases but also the transition to the annular regime. One of the first to distinguish these two sub-patterns were Hewiit and Jayanti (1993). They propose the use of churn-slug and churn-annular as the transitional patterns between the slug and the annular flow. The unstable slug is characterized by highly aerated liquid pistons trailed by gas bubbles surrounded by aerated liquid film. Most of the time the gas bubble and liquid piston structures are preserved but, sometimes, the liquid slug between neighboring bubbles may collapses at high flow rates. The falling liquid content is drained downward and eventually is intercepted by an upward liquid piston. The chock between these two streams introduces chaotic flow disturbance with an oscillatory or churn motion of the liquid in the tube followed by a loss of integrity of the elongated bubble. This regime persists until the gas flow is high enough to break down all of the slugs and distribute their content in the form of waves on annular film. The high speed mixture has gas–liquid structures several pipe diameters long. The velocity and the length of the flow structures avoid visual identification of the whole unit by naked eye due to the high velocity and also prevent to capture it in a single frame of a high speed camera due to its length. Usually only a fraction of the piston or the bubble is observable making hard the identification employing only images, one has to rely on the analysis of the line averaged void fraction's trace and its PDF. The void fraction trace oscillates from 0.2 to 0.8 but it does not show a definite range for high and low as the slug flow. The loss of integrity of the gas bubble followed by the increase of the gas content on the liquid film as well as on liquid slug prevents the signal to change from low to high in a step-wise way. Instead, intermediate values of ε, i.e. $0.4 < \varepsilon < 0.6$, happens more frequently causing the PDF values, between the two peaks, be no longer negligible, see Fig. 5.

The Semi-Annular flow is the term often used to the existing flow pattern between the unstable slug and the annular flow, Azzopardi and Hills (2003). It is considered a degenerated form of annular flow with large interfacial waves with the liquid film direction changes. A typical trace and PDF of this flow pattern is shown in
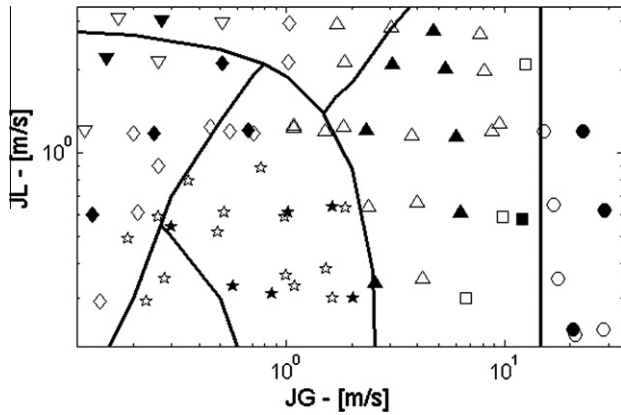
Fig. 5. The trace of ε still shows large oscillation between 0.4 and 0.9 but occurrence of the high values of ε prevails and the expected mean values range from 0.7 to 0.8. The PDF is single peaked with a large skew toward low values of ε.

The Annular flow is characterized by a core with high velocity gas–droplets mixture surrounded by a co-current liquid film. The liquid film is occasionally interrupted by disturbance waves which leaves their footprint on the time trace of ε as short duration peaks ranging from 0.4 to 0.95. The expected mean values is always higher than 0.8. The PDF is single peaked with skew toward the low values of ε, see trace and PDF in Fig. 5. Although, not observed in this work, it is added, for completeness, a second flow pattern belonging to the annular type flow: the wispy-annular flow. It is characterized by an agglomeration of liquid in the gas core causing the formation of streaks or wisps of liquid due to an increase on the liquid velocity at a given gas velocity, Hewiit and Hall Taylor (1970).

3.4. The experimental data set

Seventy-three runs with air and water superficial velocities spanning, respectively, from 0.1 m/s to 30 m/s and from 0.20 m/s to 3.0 m/s have their flow patterns identified. The data correspond to the flow conditions found at 257 pipe diameters downstream the air–water mixer and have their statistical moments displayed in Table 1 as a form to convey information regarding the line averaged void fraction PDF. The first column displays the run numbering. The second and third columns bring, respectively, the in situ superficial velocities of the liquid and gas phases, J_L and J_G. The mean, the standard deviation, the skewness and the kurtosis of

the line averaged void fraction are displayed along the 4th until the 7th column. Finally the flow patterns are labeled on the 8th column. The letters BB, SC, SS, US, SA and AA stand for bubbly, spherical cap, stable slug, unstable slug, semi-annular and annular flow patterns. The 73 data points are considered with enough variability and representativeness to apply to flow pattern identification techniques. Table 2 brings, for convenience, the percentage of occurrence of each flow pattern on the experimental data set. The flow patterns are not uniformly distributed along the six labels; 57% of the runs correspond to the stable slug and unstable slug patterns. This feature is justified because these flow patterns are likely to occur over a large range of liquid and gas velocities on the flow map, see Fig. 7 where symbols with the same shape represent the same flow pattern. The distinction between open and solid symbols is to identify the data belonging to the training and to the testing data sets to be defined on the next section.

Table 2
Percentage flow pattern occurrence on the experimental, training and testing data sets.

Flow pattern	Exp. Runs (%)		Training Runs (%)		Testing runs Runs (%)	
Bubbly flow	6	8	5	10	3	13
Spherical cap	13	18	4	8	2	9
Slug flow	20	27	9	18	4	17
Unstable slug	22	30	14	28	6	26
Semi-annular	4	5	15	30	7	30
Annular	8	11	3	6	1	4
Total	73	100	50	100	23	100

Table 1
Experimental data set. J_L and J_G are the water and the air superficial velocities. M, Std, Skw and K stand for mean, standard deviation, skewness and kurtosis of the line averaged void fraction, ε. BB, SC, SS, US, SA and AA stands for bubbly, spherical cap, stable slug, unstable slug, semi-annular and annular flow patterns.

Run #	J_L (m/s)	J_G (m/s)	M	Std	Skw	K	Flow pattern	Run #	J_L (m/s)	J_G (m/s)	M	Std	Skw	K	Flow pattern
1	1.21	0.67	0.19	0.22	1.41	3.50	SC	38	0.60	0.13	0.06	0.14	2.11	5.73	SC
2	0.36	1.00	0.57	0.38	−0.35	1.29	SS	39	1.21	0.12	0.02	0.06	3.69	16.45	BB
3	0.59	0.99	0.47	0.37	0.05	1.20	SS	40	2.22	0.15	0.04	0.03	5.66	41.88	BB
4	1.23	1.08	0.27	0.26	0.89	2.17	US	41	3.08	0.17	0.06	0.01	3.57	31.88	BB
5	0.38	1.53	0.65	0.35	−0.77	1.83	SS	42	0.61	0.21	0.10	0.19	1.50	3.53	SC
6	0.64	1.63	0.54	0.34	−0.29	1.33	SS	43	1.18	0.20	0.04	0.10	2.52	8.07	SC
7	1.20	1.51	0.34	0.28	0.52	1.59	US	44	2.16	0.26	0.06	0.05	3.27	14.6	BB
8	0.34	2.56	0.70	0.28	−1.12	2.76	US	45	3.05	0.27	0.06	0.03	4.33	26.9	BB
9	0.64	2.38	0.60	0.31	−0.60	1.69	US	46	1.20	0.55	0.11	0.19	1.29	3.00	SC
10	1.21	2.34	0.43	0.28	0.14	1.38	US	47	2.12	0.51	0.11	0.10	1.97	6.16	SC
11	0.35	4.20	0.75	0.22	−1.36	4.00	US	48	2.98	0.51	0.10	0.05	2.73	11.7	BB
12	0.66	4.00	0.67	0.27	−0.93	2.44	US	49	1.25	1.09	0.22	0.24	0.56	1.62	US
13	1.16	3.74	0.54	0.28	−0.31	1.46	US	50	2.13	1.02	0.21	0.18	1.37	3.66	SC
14	0.30	6.69	0.77	0.16	−1.19	4.90	SA	51	2.95	1.03	0.17	0.09	1.90	6.58	SC
15	0.61	6.27	0.71	0.22	−1.28	3.82	US	52	0.30	2.02	0.54	0.27	−0.95	2.44	SS
16	1.15	6.00	0.61	0.26	−0.66	1.93	US	53	0.63	1.88	0.44	0.29	−0.40	1.55	SS
17	0.58	12.07	0.79	0.16	−1.50	5.56	SA	54	1.24	1.83	0.30	0.25	0.10	1.34	US
18	1.20	8.79	0.68	0.24	−0.87	2.44	US	55	2.13	1.86	0.33	0.22	0.80	2.20	US
19	0.35	0.28	0.37	0.35	0.44	1.40	SS	56	2.92	1.72	0.25	0.13	1.51	4.77	US
20	0.33	0.57	0.43	0.37	0.16	1.20	SS	57	2.09	3.05	0.41	0.20	0.31	1.62	US
21	0.31	0.86	0.54	0.37	−0.28	1.27	SS	58	2.85	3.03	0.39	0.19	0.94	2.65	US
22	0.33	1.10	0.58	0.35	−0.49	1.46	SS	59	2.03	5.34	0.52	0.19	−0.18	1.53	US
23	0.30	1.63	0.64	0.32	−0.80	1.94	SS	60	2.78	4.75	0.47	0.19	0.41	1.76	US
24	0.59	0.26	0.27	0.32	0.84	1.93	SS	61	0.59	9.76	0.65	0.14	−1.24	5.21	SA
25	0.61	0.52	0.30	0.33	0.68	1.68	SS	62	1.28	9.47	0.66	0.16	−1.13	3.17	US
26	0.61	1.02	0.46	0.35	0.06	1.23	SS	63	1.99	8.09	0.59	0.18	−0.51	1.92	US
27	0.90	0.26	0.21	0.26	1.07	2.41	SC	64	2.69	7.71	0.56	0.18	−0.05	1.66	US
28	0.88	0.77	0.33	0.30	0.53	1.54	SS	65	0.23	20.6	0.81	0.09	−0.99	3.55	AA
29	1.18	0.25	0.17	0.21	1.42	3.42	SC	66	0.22	21.1	0.80	0.09	−0.92	3.48	AA
30	1.24	0.45	0.19	0.22	1.23	2.93	SC	67	0.35	17.6	0.76	0.10	−0.67	3.09	AA
31	1.18	0.71	0.26	0.25	0.80	2.00	SC	68	0.65	16.7	0.79	0.09	−1.48	6.93	AA
32	0.29	0.23	0.23	0.32	0.97	2.23	SS	69	1.2	15.2	0.78	0.11	−1.94	7.51	AA
33	0.54	0.30	0.26	0.32	0.88	2.00	SS	70	2.09	12.4	0.72	0.14	−1.18	3.58	SA
34	0.49	0.19	0.23	0.31	0.97	2.19	SS	71	0.23	28.3	0.87	0.06	−1.09	3.77	AA
35	0.52	0.49	0.30	0.35	0.65	1.60	SS	72	0.62	28.8	0.84	0.07	−1.04	4.67	AA
36	0.79	0.36	0.22	0.28	1.01	2.26	SS	73	1.20	22.8	0.82	0.09	−1.94	8.57	AA
37	0.29	0.14	0.10	0.20	1.67	4.26	SC								

Fig. 7. Flow map having the water and the air superficial velocities on the y and x axes. Solid lines represent the boundaries defined by Taitel et al. (1980). Open and filled symbols represent data belonging to the training and to the testing data sets, respectively. Symbols: ∇ – BB; $\diamond$ – SC; $\star$ – SS; $\triangle$ – US; $\square$ – SA; $\circ$ – AA (bubbly, spherical cap, stable slug, unstable slug, semi-annular and annular).

The consistency of the flow patterns labels is checked against the flow map given by Taitel et al. (1980) in Fig. 7. To establish a comparison it is necessary to reduce the six identified patterns to the four patterns proposed by Taitel et al. (1980), i.e., the bubbly and spherical cap patterns correspond to Taitel's bubbly flow and the unstable slug and semi-annular patterns correspond to the Taitel's churn flow. Considering this correspondence among flow pattern labels it is observed, in overall, a good agreement between the experimental data and the map. As expected, the misclassifications happen at the boundaries of the patterns where the identification criteria become fuzzy. In particular the region where misclassification rate is higher rests where the three boundary lines merge.

The experimental data consistency is also observed on the evolution of the line averaged PDF as the water and the air velocities change as seen on Fig. 8. The x and y coordinates are, respectively, the air and the water superficial velocities. The x and y position where the PDF lays correspond, approximately, to the same superficial velocities as indicated by the x and y axes. Consider, for example, the effect of the increase on the air superficial velocity. At low air velocities is observed the spherical cap regime displaying a PDF single peaked with positive skew, #37. As the air velocity increases the pattern changes to the slug flow and further on it changes to the unstable slug, both with bimodal PDFs, see points #20 and #8. Additional increases on the air velocity causes the semi-annular and the annular flow regimes corresponding to single peaked PDFs with negative skew, points #14 and #71. The increasing of the water velocity always reduces the line averaged void fraction but its effect on the PDF depends on the air velocity. For example, at the lower range of J_L and J_G it is observed the spherical cap regime, point #37. As the water velocity increases the PDF skewness is progressive reduced and eventually approaches a symmetrical distribution found in the bubbly regime, point #40. Alternatively, one can also build a figure, similar to Fig. 8, employing the first four statistical moments and reach similar conclusions.

3.5. Training and test data sets

Before developing the flow pattern identification techniques it is convenient to define the training and the testing data sets. The training set is the source of knowledge to the identification techniques; it demands a large number of elements to create a representative base. Complementary, the test set is used to assess the performance of the identification techniques. The original data set is split into two sub-sets with approximately 70% and 30% of the data corresponding to the training and test sets, respectively. There are no data repetition between the two sets in such a way that the union of the two sub-sets result on the original data set.

The training and test sets have, respectively, 50 and 23 elements carefully chosen to guarantee the variability and representativeness of the original data. Both sets are identified by their run
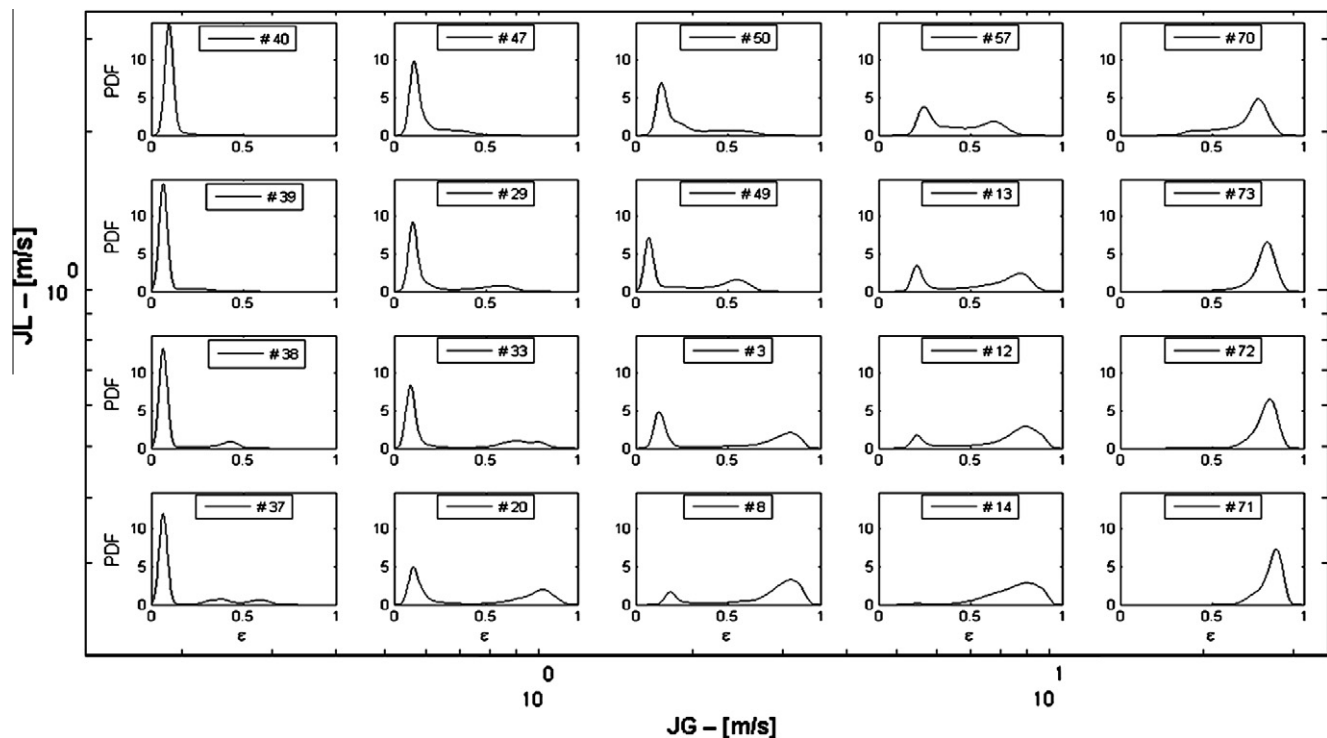

Fig. 8. Evolution of the line averaged void fraction PDFs as the water and air superficial velocities change along the flow map.

Table 3
Training and testing data sets numbering, see data characterization on Table 1.

Training data set numbering, #					Testing data set numbering, #		
2	18	32	46	61	1	29	65
3	19	34	48	62	6	33	72
4	22	35	49	63	8	38	73
5	23	36	50	64	10	40	
7	24	37	51	66	15	45	
9	25	39	53	67	16	47	
11	27	41	54	68	17	52	
12	28	42	55	69	20	57	
13	30	43	56	70	21	59	
14	31	44	58	71	26	60	

numbering on Table 3 and exhibit the same percentage of occurrence of each flow pattern which also coincides, approximately, to the one found on the original experimental data set, see Table 2. The representativeness between the two data sets is appreciated by superposing the PDF curves belonging to each set and observing the similarity between the curves' envelope shown in Fig. 9.

4. Flow pattern identification techniques

The flow pattern identification techniques map an objective flow indicator to a flow pattern label, see schematic on Fig. 10. Two types of objective flow pattern indicators are used: the first four statistical moments and the PDF, both based on the instantaneous readings of line averaged void fraction. The use of one indicator or the other is defined along the context. The output is the classification of the given objective flow indicator to a corresponding flow pattern label.

The mapping procedures demand a knowledge base, KB, necessary to the learning stage of the identification techniques. The KB is formed either by a human specialist or with the aid of clustering algorithms which group the data accordingly to topological similarities.

Two types of flow pattern identification techniques are employed: the artificial neural networks and expert systems. The following sections describe in detail the adopted procedures to the establishment of the knowledge base and the identification techniques.

4.1. Knowledge base, KB

The success of the identification techniques relies on how representative is the knowledge base regarding the data universe. If the knowledge base does not convey representative information of the data or even worse, if it has conflicting information, the outcome of the identification techniques may be impaired. The employed KB consists of 50 data belonging to the training set displayed on Table 3. Each data must be associated to a flow pattern label. If this procedure is done by a human specialist the KB
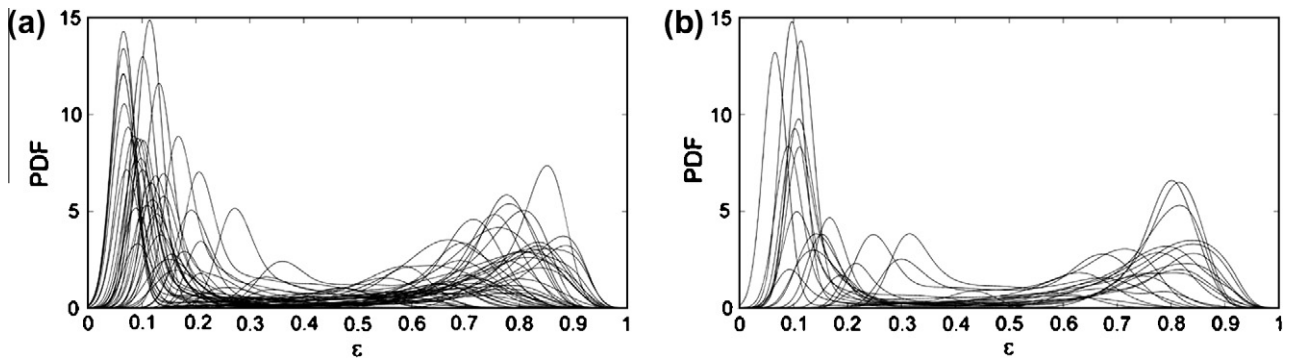

Fig. 9. Superposition of the PDF́s shapes (a) training data set with 50 curves and (b) testing data set with 23 curves.
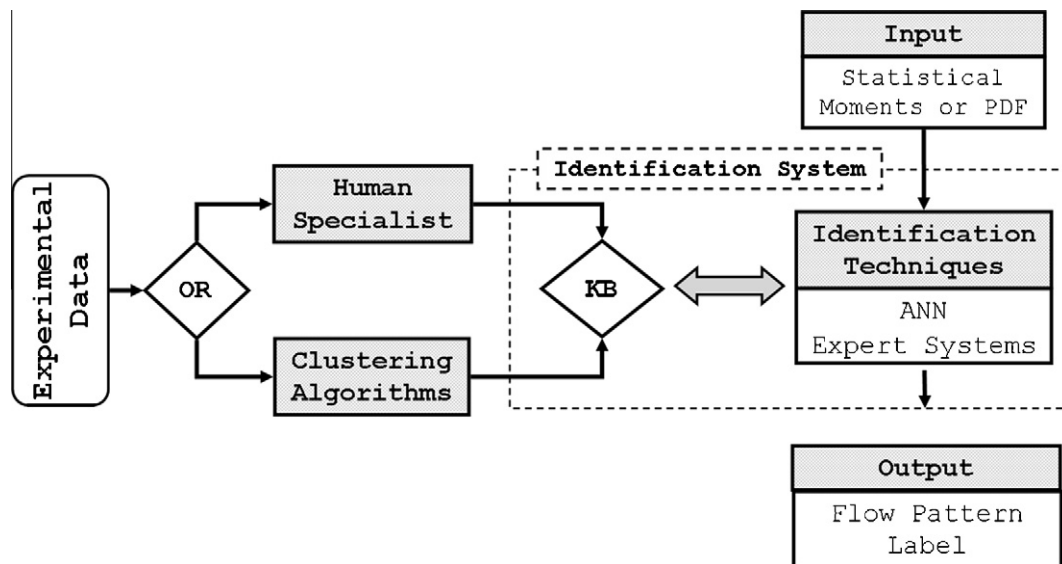

Fig. 10. Schematic representation of the identification technique and the knowledge base.

is referred to KB-HS. On the other hand, if the data are first grouped by a clustering algorithm and in a second step each group is labeled by a human specialist it is referred to KB-CA. There are differences between these two procedures, the most apparent is on the fact that the human specialist procedure is intrinsically subjective while the KB formed with the aid of clustering algorithms is free from subjective criteria. The next sections brief these procedures.

4.1.1. Knowledge base based on human specialist – KB-HS

A KB-HS is based on a subjective evaluation of the data similarities. The analysis is not based on a single parameter. The human specialist searches for similarities among the temporal series of the line averaged void fractions and the associated PDFs, cross correlate this information with the flow descriptors and with the expected qualitative behavior of the void fraction value. The selected 50 data points are identified on Table 3, labeled by a human specialist on Table 1, displayed on flow map in Fig. 7 and have the percentage of occurrence of each pattern shown on Table 2. The disadvantage of this procedure is the degree of subjectiveness inherent to the specialist judgment. It also demand large amount of time to properly classify since the information belonging to each data has to be analyzed individually as well as in clusters to properly label each point to a specific flow pattern.

4.1.2. Knowledge base based on clustering algorithm – KB-CA

The data clustering algorithms group the objective flow pattern indicators by establishing topological similarities. These techniques are often called as non-supervised because they are capable to form knowledge bases free from subjective judgment. The human specialist's function is to associate each group to a specific flow pattern, but the data clustering is performed autonomously. Fig. 11 represents the formation of a KB-CA, based on PDFs, in two steps. The first step clusters the PDF curves into six groups based on existing topological similarities among the PDFs. This task is performed by an autonomous clustering algorithm. Step II associates each cluster to one of the six flow pattern labels. This task is done by a human specialist.

Three clustering algorithms are employed: Kohonen self organized map, K-means and Fuzzy C-means which are represented

as SOM, KM and FCM, respectively. A short description of these techniques follows.

K-means – KM – is a simple unsupervised learning algorithm to solve the clustering problem based on the minimum Euclidian distance from a given curve to another curve which represents the cluster's centroid. The procedure classify a given curve set into k clusters, here k equals to six representing the flow patterns. The main point is to define k centroids, one for each cluster; it is done iteratively. The initial guesses for the k centroids is an arbitrary choice of k curves which are as distinct from each other as possible. The next step is to take each curve in a given curve set and connect to the nearest centroid. At the end of this procedure will be formed the first k groups with similar curves. A new centroid is determined and the whole procedure is repeated in a loop until a convergence criteria is reached (MacQueen, 1967).

Self Organized Maps – SOM – is an ANN which preserves the data similarities employing a competition strategy. The main objective of the self organized maps is to group topologically similar data (Kohonen, 1982). The Euclidian distance is used as a measure of similarity among the vectors. The non-supervised learning stage consists of weight adjustments based on the input data similarity. The employed SOM is a two-dimensional ANN with two neurons' layers. The output layer has six neurons corresponding to the chosen flow patterns. The winner takes all strategy activates only one neuron, detailed information is found in Kohonen (2001).

Fuzzy C-means – FCM – solve the clustering problem based on fuzzy criteria to determine the minimum Euclidian distance from a given curve to another curve which represents the cluster's centroid. Generally speaking it is a fuzzy K-means. The K-means method associates each curve to a specific cluster, i.e., the classified curve has no pertinence degree to neighboring clusters. Sometimes this classification strategy does not work well if the transitions from one type of cluster to the other occur continuously as it happens with the flow patterns. The FCM overcomes this deficiency employing fuzzy logic to establish the degree of pertinence of each curve to the k groups. The method defines a pertinence matrix U where the elements $u_{i,j}$ represent the degree of pertinence of curve i to the j group. The degree of pertinence of the FCM method conveys more information to the output than the KM method. As an
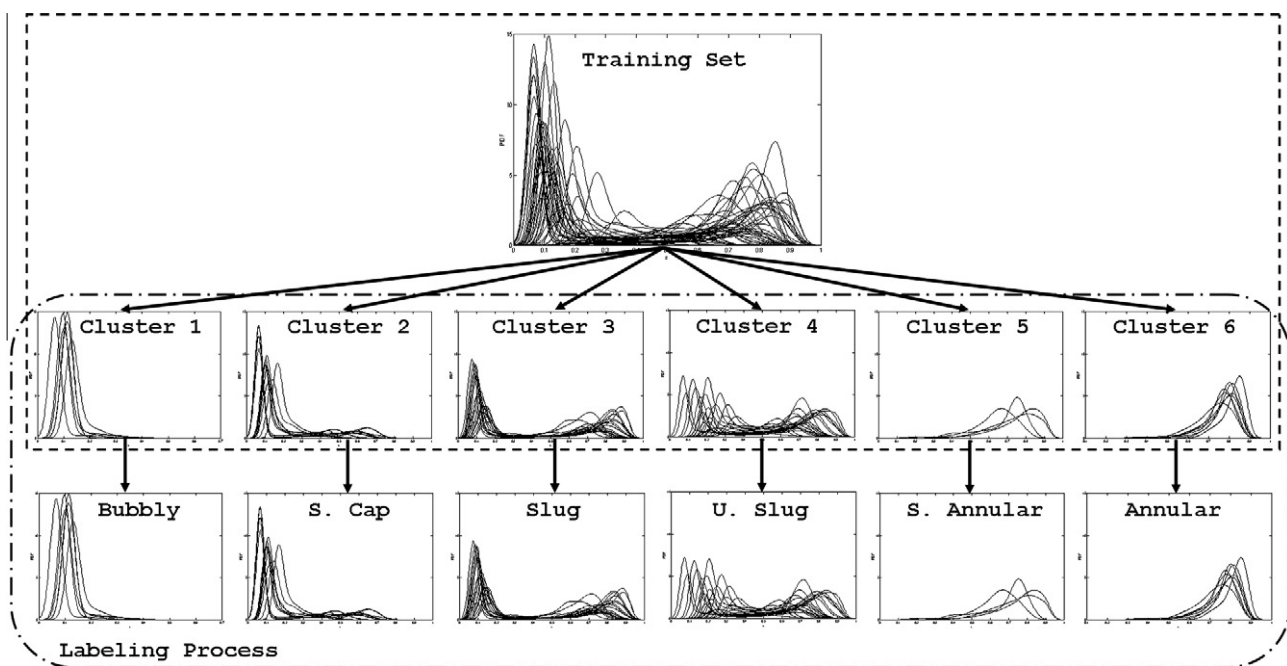

Fig. 11. Formation of a knowledge base assisted by clustering techniques. Step I – PDF clustering by autonomous algorithm. Step II – group labeling by human specialist.

example consider the classification of a given PDF. The KM method classify the curve as belonging to the bubbly flow pattern but the FCM output would assign, for example, 0.7 to the bubbly flow pattern and 0.3 to the spherical cap pattern. The pertinence degree of single PDF to multiple flow patterns gives information about transitional zones. The FCM's theory and implementation details are in Bezdek (1981) and He (1998).

4.2. Flow pattern identification techniques

The flow pattern identification techniques are supervised systems which have a learning stage based on the knowledge base, see schematic in Fig. 10. The employed supervised techniques include artificial neural networks and expert systems which are detailed on the next sections.

4.2.1. Artificial neural networks – ANN

Three types of ANN are applied to flow pattern identification: the multiple layer perceptron, MLP; the radial base function, RBF and the probabilistic neural network, PNN. The ANNs share some similarities which will be described beforehand. The input vectors may be either the statistical moments or the PDFs. The former requires ANN with four neurons at input layer while the last uses 300 neurons. Certainly the last number can be reduced without much loss of information using, for example, principal component analysis (Jolliffe, 1986), but the optimization of the input dimension was considered out of the scope in this work. This subject is approached in an alternative way in Section 5.3. The ANN's output layer can have a single or multiple neurons, SO or MO, respectively.

The ANN with single or multiple neurons at the output layer has its value within 0 and 1 normalized on [0, 1] by applying the logsig function. Fig. 12 represents schematically the ANNs with SO and MO architectures having as input vectors the PDFs. The correspondence of the output layer's neurons to the flow pattern label is also given in the figure. For SO architecture the output is divided into six intervals having each interval corresponding to a flow label. The MO architecture has each output neuron corresponding to a flow label. Specific features of MLP, RBF and PNN are briefed on the following paragraphs.

Multi-layer Perceptron ANN-MLP – is frequently employed for pattern recognition tasks. The neurons are connected in a feed-forward fashion via multiplicative weights and arranged in a weight matrix W. The MLP must be trained with the KB data to find the appropriate values for the elements in matrix W, given the number of neurons in the hidden layer. The employed learning algorithm is the error back-propagation, Rumelhart et al. (1986). More details of MLP are found in Bishop (1995).

Radial Basis Function ANN-RBF – are particularly designed to non-linear function approximations. Originally proposed by Broomhead and Lowe (1988), they have three layers. The neurons

within each layer are fully connected to the neighboring layers similarly to an ANN-MLP. The hidden layer is defined by a set of radial basis functions which give the name to this type of ANN. The learning stage is equivalent to the fitting of a surface to a set of data in a multi-dimensional space constrained by a statistical criterion. The ANN-RBF are capable to map non-linear functions with just one hidden layer which is an advantage in regard to the required number of hidden layers in ANN-MLP, Bishop (1995). This superior performance is not always achieved due to the algorithms to finding the optimum number of hidden neurons as well as their amplitudes and centers which frequently settle in local sub-optimum configurations, Bishop (1995).

Probabilistic Neural Networks ANN-PNN – are known for exhibiting a high learning level which result in a classification rate as good or superior to the ANN-MLP. Originally developed by Specht (1990), the ANN-PNN is based on Bayes decision strategy and on Parzen's method of PDF approximation, Friedman et al. (1997). The ANN-PNN act like a feed forward network similar to the ANN-MLP with four neuron layers with radial basis Gaussian functions. The similarities to the ANN-MLP extend to: capability of non-linear mapping, generalization character and parallelism. One of the advantages of the ANN-PNN is in the estimate of the pertinence degree upon which its decision is based. One of the disadvantages is the fact that ANN-PNN demand more computational resources than ANN-MLP.

4.2.2. Expert systems ES

Expert system is an algorithm that attempts to reproduce the performance of one or more human experts in a specific problem (Hayes-Roth et al., 1983). A wide variety of methods can be used in expert systems; however, the most frequently employed are the so-called conditional structures of the type "if-then-else" connected and interlinked with some objective. Each structure form a rule and the rules' combination create the inference process of the expert system model. The set of rules are capable to store several types of information and can represent many problems in several applications. The inconvenience of this methodology is the rule creation and encoding process that, depending of the problem, can became cumbersome (Giarratano and Riley, 1994 and Waterman, 1986).

The input vector is represented by S_j. It is proposed an inference process in two stages. The first stage determines the Euclidian distance, $^1{}_i$, from the input vector, S_j, to each vector $P_{i,j}$ belonging to the KB, as shown by

$$\Delta_i(P_{i,j}, S_j) = \sqrt{\sum_{j=1}^{300}(P_{i,j} - S_j)^2}; \quad 1 \leqslant j \leqslant 300. \tag{6}$$

The indexes i and j represent, respectively, the number of vectors and the vector dimension. The range of index i is $1 \leqslant i \leqslant 50$ due to the size of the training set; considering the PDFs as the input
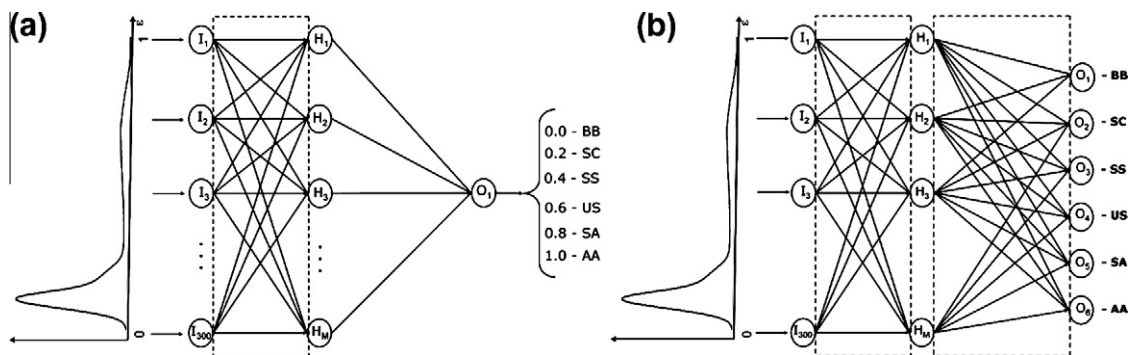

Fig. 12. ANN schematic representation. Input layer having the PDFs. Output layers with (a) single neuron and (b) multiple neurons.
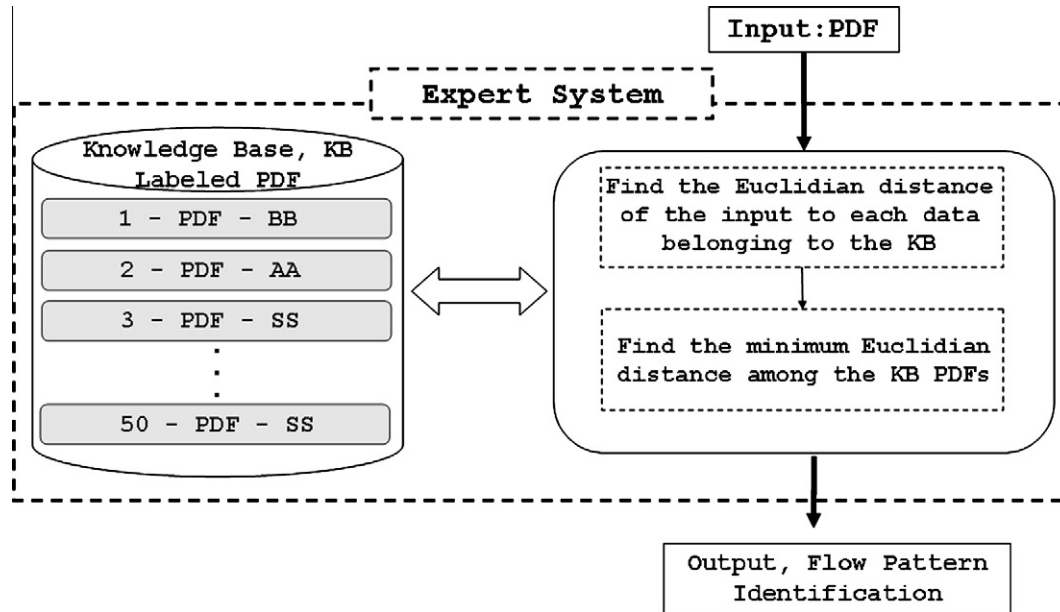
Fig. 13. Schematic representation of the expert system employing as input vector the PDFs.

vector the range of index j becomes $1 \leqslant j \leqslant 300$. The second stage determines the minimum of $^{1}{}_{i}$ as a way to find the most similar vector $P_{i,j}$ to the input S_j. Due to the geometrical similarity between the two vectors the method infers that both vectors have the same flow pattern, i.e., S_j receives the same flow pattern label of the $P_{i,j}$ vector which resulted on the minimum of $^{1}{}_{i}$. A schematic representation of the expert system having as input vectors the PDFs is in Fig. 13 including the inference set of rules and KB.

4.3. Summary

The developed identification techniques are associated with input vectors and knowledge bases which need to be properly identified for further references. This section addresses this issue by listing the employed techniques.

Four methods are employed to establish the knowledge base: one is a KB-HS and the three others are based on KB-CA. These methods resulted in distinct knowledge bases which are identified in Table 4.

Three types of ANN are used, each one with two architectures: single and multiple output neurons resulting in a total of six distinct ANN's. For comparison purposes the ANNs are all linked to a single knowledge base, the KB-1. Additionally there are the expert systems which have the same inference algorithm, see Section 4.2, but are associated with four distinct knowledge bases. The number of identification systems amounts to 10 if one considers the distinct principles, architectures and knowledge base associations. All configurations employ as input vectors the PDFs of the line averaged void fraction. The exception applies to an additional case where an ANN-MLP with multiple outputs has as input the statistical moments. Table 5 summarizes the identification techniques, input vectors and knowledge bases.

Table 4
Methods employed to the knowledge base formation.

#	Name	Short name	Knowledge base
1	Human specialist	HS	KB-1
2	Kohonen self org. map	SOM	KB-2
3	K-means	KM	KB-3
4	Fuzzy C-means	FCM	KB-4

5. Results

The performances of the clustering algorithms and identification techniques are gauged in two ways. The first measures the percentage of right identification achieved by a specific identification technique, PRIT, when submitted to the testing set. The second gives the percentage of right identification received by a specific data point, PRIP, when submitted to all identification techniques. The PRIT figure gives an idea of how accurate the identification technique is while the PRIP show how a specific data point is predicted by different identification techniques. The PRIT and PRIP figures are evaluated accordingly to:

$$PRIT(k) = 100 \sum_{i=1}^{n} V_{i,k} \quad \text{and} \quad PRIP(i) = 100 \sum_{k=1}^{m} V_{i,k}, \tag{7}$$

where the indexes i and k identify, respectively, a data point and a identification technique while V_{ik} can be 1 or 0 if the identification of the ith point employing the kth technique is right or wrong, respectively. Considering, for example, the first 10 identification techniques shown in Table 5 the testing set has $n = 23$ and the identification methods have $m = 23$ which result in spanning intervals of $1 \leqslant i \leqslant 23$ and $1 \leqslant k \leqslant 10$, respectively.

The next three sections explore the results of the clustering algorithms, flow pattern identification techniques and the influence of downsizing the input data.

5.1. Clustering algorithms

This section presents the classification of the training data set into six groups using the KM, SOM and FCM clustering algorithms. The inputs are the PDF of the line averaged void fraction. The clustering algorithms were tested several times to assure repeatability better than 95%. These algorithms were implemented in a 2.2 GHz dual core machine using MATLAB© R14 V.7.0|SP3. The convergence was achieved in less than 1000 cycles with approximately 2 s of cpu.

The resultant flow pattern classification is on Table 6. The first column displays the experimental run. The second column displays the classification given by the human specialist. The next three columns show the labels obtained by KM, SOM and FCM algorithms.

Table 5
Flow pattern identification techniques, input vectors and associated knowledge base. SO and MO stands for single and multiple output layer; SM means statistical moments.

#	Type/name	Input vector	Knowledge base
1	ANN-MLP-SO	PDF	KB-1
2	ANN-MLP-MO	PDF	KB-1
3	ANN-RBF-SO	PDF	KB-1
4	ANN-RBF-MO	PDF	KB-1
5	ANN-PNN-SO	PDF	KB-1
6	ANN-PNN-MO	PDF	KB-1
7	ES-1	PDF	KB-1
8	ES-2	PDF	KB-2
9	ES-3	PDF	KB-3
10	ES-4	PDF	KB-4
11	ANN-MLP-MO	SM	KB-1

It is noteworthy to observe on Table 6 that among the mismatched cases there are 17 cases common to all algorithms, i.e., the three algorithms show the same flow pattern which is distinct of the flow pattern indicated by the human specialist. As an example run #50 is classified as SC pattern but all three algorithms classify the same point as SS pattern. Also run #70 is found to be SA pattern while the three algorithms indicate AA pattern. The additional triple mismatched points are: {24, 25, 5, 35, 36, 4, 7, 54, 55, 56, 58, 49, 63, 64, 39}. With the aid of Table 1 it is possible to place these points on the flow map, see Fig. 7, and identify two sub-data sets: one characterized by points which lay on the transitional boundaries {4, 7, 24, 36, 49, 50, 53, 55, 58, 63, 64, 70} and the other characterized by non-transitional points {5, 25, 35, 39, 56}.

The factors which lead to the mismatches on transitional points are:

(a) The three algorithms search for similarities among the data set based on the minimum Euclidian distance between vectors. This strategy is successful when the features of each cluster are clearly distinguishable. But, the flow pattern features do not change in a step-wise way from on pattern to the other; on the contrary, the features change continuously making it harder to the clustering algorithms to work with the transitional points.

(b) The human specialist knowledge base, KB-1, is built based on subjective criteria which, intrinsically, impart some uncertainty on the classification process that is difficult to gauge. To remedy this inherent deficiency the data is extracted from an experimental setup largely employed in the literature: a vertical one inch pipe with an air–water mixture flowing upward. The experimental flow pattern data displays a favorable comparison with the flow map predictions as well as with the reported data on the literature, see Section 3.4;

(c) Clustering techniques are sensitive to the number of groups, Juliá et al. (2008) and Lee et al. (2008). Maybe fewer groups, for example: bubbly, slug, churn and annular see Taitel et al. (1980), may result in an improvement on the methods performance. The techniques are also sensitive to the number of samples of each pattern. Imbalanced data set may favor some specific groups than the others. Unfortunately the training data set has nearly 60% of samples for SS and US patterns and 13% for SA and BB patterns. Significant improvements on the outcomes are observed in tests where the training data set is trimmed to a balanced number of samples to each flow pattern label.

(d) Finally, the number and the choice of the experimental runs to build the training set may have an impact on the clustering methods. Despite of the attempt to have the experimental data uniformly distributed on the flow map, it is possible that data points laying on distinct areas of the flow map may result in better

performances. Furthermore no data swap between the training and testing data set was done. This task would increase in many orders the analysis work involving the three clustering methods.

Despite of the plausible causes justifying the existence of mismatch at transitional points they cannot support the existence of mismatches on non-transitional points. The misclassifications are inconsistencies of the methods very likely associated to items (a) and (c). For completeness, the results in Table 6 show a percentage of right identification for the KM, SOM and FCM algorithms of 46%, 50% and 62%, respectively. These scores apply to the 50 PDFs belonging to the training data set.

This analysis, although limited, is not favorable to the clustering methods as a tool to identify the six flow patterns. This result can be enhanced if the algorithms still distinguish six groups but the results are shown in a reduced number of flow patterns. The choice of six flow pattern was intentionally used as a form to explore the transitional points. But there are many other forms to form flow pattern groups; see for example a short review on the literature from 1936 up to 1987 for the proposed flow patterns labels in Samaras and Margaris (2005). This work explores the use of two of them. The first consists of the four flow patterns proposed by Taitel et al. (1980): the bubbly, the slug, the churn and the annular flow patterns. The correspondence among the used six flow patterns to the Taitel's flow patterns was already described in Section 3.4. The identification of only four flow patterns increases the percentage of right answers to 80%, 82% and 88% when considering the KM, SOM and FCM algorithms, respectively. The second choice considers only three flow patterns: the bubbly, the intermittent and the annular flow patterns. The equivalence among the six flow patterns to this new partition is as follow: the bubbly flow remains the same for both; the intermittent flow encompasses the spherical cap, stable slug and unstable slug flows and finally the annular flow corresponds to the semi-annular and annular flows. The identification of three flow patterns rises the percentage of right identifications to 88%, 92% and 96% considering, respectively, the algorithms: KM, SOM and FCM. Reducing the number of flow patterns greatly enhance the algorithms performance by relaxing the need to classify transitional points. In all three scenarios the FCM algorithm had a slightly better performance than the other two algorithms.

5.2. Flow pattern identification techniques

Expert systems and ANN are employed as flow pattern identification techniques, both using as input vectors the PDFs. The expert systems, for being conceptually simple, do not have any particular set up detail to be declared but some specific set up features of the ANNs are given on the following lines. The ANN-MLP has the number of neurons on the hidden layer and the momentum term estimated through an extensive search on the {5, 20} and {0.01, 0.99} domains, respectively. Furthermore, the bounds for the number of neurons were found employing the Baum-Haussler metric (Baum and Haussler, 1989). The initial learning rate of the weights was of 0.001. During each epoch a one-dimensional search was conducted to get the next weight value (Groot and Würtz, 1994 and Bromberg and Chang, 1992). The ANN-RBF and ANN-PNN were built with six neurons or centers on the hidden layer. These neurons were estimated through the FCM clustering algorithm applied to the training data set. The learning stage of all ANN was performed before 1000 epochs with a convergence time always less than 5 s. During the testing stage, the flow pattern identification was achieved in less than 50 ms. The procedures were setup in a 2.2 GHz dual core machine using MATLAB© R14 V.7.0|SP3.

The results of the identification techniques are shown on Table 7. The letters R and W implies a right or wrong identification. The

Table 6
Clustering algorithms results having the PDFs as input vectors.

Run #	Specialist	KM	SOM	FCM	Run #	Specialist	KM	SOM	FCM
27	SC	SC	SC	SC	9	US	US	US	US
42	SC	SC	SC	SC	11	US	US	US	US
31	SC	SS	SS	SS	12	US	US	US	US
37	SC	SC	SC	SC	13	US	SA	SS	US
30	SC	SC	SC	SC	18	US	US	US	US
43	SC	SC	SC	SC	54	US	SS	SS	SS
46	SC	SC	SC	SC	55	US	SS	SS	SS
50	SC	SS	SS	SS	56	US	SS	SS	SS
51	SC	BB	SC	SC	58	US	SS	SS	SS
2	SS	US	SS	SS	49	US	SC	SC	SC
3	SS	SS	SS	SS	62	US	AA	AA	SA
34	SS	SC	SC	SS	63	US	SA	SA	SA
19	SS	SS	SS	SS	64	US	SA	SA	SA
32	SS	SC	SC	US	14	SA	US	US	SA
22	SS	US	US	SC	61	SA	SA	SA	SA
23	SS	US	US	SS	70	SA	AA	AA	AA
24	SS	SC	SC	SC	66	AA	AA	AA	AA
25	SS	SC	SC	SC	67	AA	AA	AA	AA
28	SS	SS	SS	SS	68	AA	AA	AA	AA
5	SS	US	US	US	69	AA	AA	AA	AA
35	SS	SC	SC	SC	71	AA	AA	AA	AA
36	SS	SC	SC	SC	39	BB	SC	SC	SC
53	SS	SA	SA	SS	41	BB	BB	BB	BB
4	US	SS	SS	SS	44	BB	BB	BB	BB
7	US	SS	SS	SS	48	BB	BB	BB	BB

first and second columns have the run identification and the flow pattern label. The outputs are along 3rd to the 12th columns. The 13th column displays the percentage of right identification per point, PRIP, while at the table's last line is the percentage of right identification per method, PRIT.

All expert systems, ES-1 thru ES-4, employ the same inference principle but distinct knowledge bases, see definitions on Table 4. Despite of the differences on the KB, the expert systems exhibited mismatches only for the intermittent patterns: SC, SS and US. In particular for ES-1 system the mismatches occurred at transitional points. On the other hand, the ES-2, ES-3 and ES-4 systems exhibited triple mismatches on transitional and non-transitional points, see data {33, 31, 15}. The observed percentage of right iden-

tification per method is of 91%, 70%, 74% and 78% for the ES-1, ES-2, ES-3 and ES-4, respectively. The method's percentage of right identification is sensitive to the choice of KB. The highest score come with ES-1 system due to the use of a KB based on human specialist. The use of clustering algorithms to assist the process of creating the knowledge base resulted in a poorer performance. This result was already expected since the clustering algorithm did not perform well to cluster the 50 PDFs of the training data set. But, at the same token, it surprises because the performance of the ES-2, ES-3 and ES-4 systems stayed above the performance of the clustering algorithms. In fact, the percentage of wrong identifications delivered by the clustering algorithms during the KB formation does not cause, necessarily, large disturbances on the performance

Table 7
Results of the flow pattern identification techniques having the PDFs as input vectors.

Run #	Label	ES-1	ES-2	ES-3	ES-4	MLP SO	RBF SO	PNN SO	MLP MO	RBF MO	PNN MO	PRIP (%)
40	BB	R	R	R	R	R	R	R	R	R	R	100
45	BB	R	R	R	R	R	R	R	R	R	R	100
1 T	SC	R	R	R	R	W	R	R	W	R	R	80
29	SC	R	R	R	R	R	R	R	R	R	R	100
38	SC	R	R	R	R	W	R	R	R	R	R	90
47	SC	R	W	R	R	R	R	R	R	R	R	90
33	SS	R	W	W	W	R	R	R	R	R	R	70
21	SS	R	W	W	W	R	R	R	R	R	R	70
26	SS	R	W	R	R	R	R	R	R	R	R	90
20	SS	R	R	R	R	R	R	R	R	R	R	100
6	SS	R	W	R	R	R	R	R	R	R	R	90
52	SS	W	W	R	R	W	W	W	R	R	R	50
8	US	W	R	W	W	R	R	R	R	R	R	70
10	US	R	R	W	R	R	R	R	R	R	R	90
15	US	R	W	W	W	W	W	W	R	R	R	40
16	US	R	R	W	W	R	R	R	R	R	R	80
59	US	R	R	R	R	R	R	R	R	R	R	100
57	US	R	R	R	R	R	R	R	R	R	R	100
60	US	R	R	R	R	R	R	R	R	R	R	100
17	SA	R	R	R	R	R	W	R	R	R	R	90
65	AA	R	R	R	R	R	R	R	R	R	R	100
72	AA	R	R	R	R	R	R	R	R	R	R	100
73	AA	R	R	R	R	R	R	R	R	R	R	100
PRIT (%)		91	70	74	78	83	87	91	96	100	100	

of expert systems when they are submitted to the testing data set. This is supported by the fact that the KB and the testing set have distinct PDFs. Furthermore, the former has a greater number of points laying on transitional zones which increases the odds of mismatches. The expert systems, despite of being simple, have performance comparable to single output ANNs if the KB-1 is employed.

The ANN with single output neuron is the next category to be analyzed. The percentage of right identification per technique is of 83%, 87% and 91% for MLP, RBF and PNN, respectively. For ranking purposes it is considered that the three techniques have similar performance. The small differences among the techniques might result from the number of samples where the ANN were trained and tested. The mismatches occurred at transitional points.

Finally, the last category to be analyzed is the ANNs with multiple outputs. The percentage of right identification per technique is of 96%, 100% and 100% for MLP, RBF and PNN. Compared with the previous techniques, the ANNs with multiple outputs have superior performance. The ANN-MLP misidentified only the point #1 which lay on a transitional zone. The RBF and PNN identified correctly the 23 points of the testing base. The performance of these three techniques are also considered equivalent. Due to its superior performance the ANN with multiple outputs are recommended for flow pattern identification.

The analysis of the percentage of right identification per point shows points {52, 15} as having the lowest scores, 50% and 40%, respectively. These points are identified as transitional points laying between SS-US and US-SA patterns, respectively. Their existences reassure the difficulties that these techniques have to identify transitional points.

The outcomes from the identification techniques are also analyzed considering the percentage of right identification per flow pattern. Table 8 shows this information by displaying on the first column the flow patterns and on the subsequent columns the identification techniques. The last column displays the averaged score per flow pattern. The figures correspond to the percentage of right identification considering the number of testing samples to the given flow pattern. The Expert systems and the ANNs with single output have the lowest identification scores to the SS and US patterns. Two factors contribute to the lowest scores. The first is because the SS and US patterns are similar. The second factor is related to the lack of proportionality on the testing data set. The SS and US patterns correspond to nearly 60% of the whole data set. On the other hand, ANNs with multiple outputs have no identification problems.

5.3. Downsizing input data to flow pattern identification

The use of PDF as input vectors with 300 dimensions may result in redundancy of information. Instead of searching for an optimized input vector size it was decided to explore the first four statistical moments as the new input vectors.

The use of the first four statistical moments is based on the fact that they convey information regarding the appearance of the PDF as well. The mean provide information on the location. The standard deviation gives the variability or dispersion. These first two moments are often recognized as scale parameters because they are related to the shift and stretching/shrinking, a typical function of scale parameters. The third and fourth moments are associated with the shape of the distribution. The skewness is related to the lack of symmetry of a PDF while kurtosis is associated with the "peakedness" of the PDF.

Based on this heuristic reasoning, an ANN-MPL is implemented having $4 \times 10 \times 6$ neurons at the input, hidden and output layers, respectively. The inputs are the first four statistical moments and the output are the flow patterns labels. The training and testing data sets are the same defined on Table 3 but instead of using PDF they employ the statistical moments defined on Table 1. The learning rate and the momentum term are of 0.03 and 0.6. The training stage has 1000 epochs with a convergence time less than 1 s.

The outcome of the ANN-MLP with multiple outputs when submitted to the testing data set achieved 100% of right identifications. The result show that the first four statistical moments convey equivalent information to the ANN as the PDFs do with the advantages of using a simpler ANN and avoiding the need of pre-processing the input vectors to render the PDF.

6. Conclusions

The clustering algorithms have, in average, 53% of right identifications to group the training data set into six flow patterns. This poor performance is due to the inability of the clustering algorithms to handle transitional data points. The algorithms' performance improves when the number of identified flow patterns is reduced. For example, if one chooses to classify only three flow patterns: the bubbly, the intermittent and the annular flow, the average of the percentage of right identification rises to 92%. They are useful tools to assist the formation process of the knowledge base having in perspective that their performance decreases as the number of flow patterns increases.

As far as the identification methods are concerned, the ANN's proved to be an efficient tool to flow pattern identification. The best results are achieved for ANN architecture with multiple outputs. The tested ANN configurations, MLP, RBF and PNN exhibited equivalent performance with percentage of right answers ranging between 96% and 100%. The expert systems are conceptually simpler than the ANN and still have a performance equivalent to the ANN with single output. Like the ANNs the expert system demands a knowledge base which in turn has an influence on the method's performance. The influence of the knowledge base on the performance of the expert system was explored. The best results come from knowledge base build by a human specialist. The knowledge base assisted by clustering algorithms result in expert systems with poorer performances. In overall the expert systems are promising tools to flow pattern identification due to its conceptual simplicity, development cost and computational speed.

Table 8
Percentage of right identification per flow pattern and per technique having the PDFs as the input vector.

Flow pattern	ES-1	ES-2	ES-3	ES-4	MLP SO	RBF SO	PNN SO	MLP MO	RBF MO	PNN MO	Mean
BB	100	100	100	100	100	100	100	100	100	100	100
SC	100	75	100	100	50	100	100	75	100	100	90
SS	83	17	67	67	83	83	83	100	100	100	78
US	86	86	43	43	86	86	86	100	100	100	82
SA	100	100	100	100	100	0	100	100	100	100	90
AA	100	100	100	100	100	100	100	100	100	100	100

Finally, the success of the developed flow pattern identification system rests on the balanced assemblage among measuring device, signal processing and identification technique. The use of the resistivity probe with a relative output voltage linearly proportional to the line averaged void fraction resulted in a good objective flow pattern indicator. This characteristic seems to be a decisive factor because the use of the PDFs or the first four statistical moments is equivalent as far as the mapping procedure is concerned. Furthermore, the identification is well accomplished with ANN with multiple neurons at the output layer regardless of the ANN's principle (MLP, RBF or PNN). The application of the statistical moments as input vector is recommended for being simple to extract and also easy to set up an identification system based on ANN.

Acknowledgements

References

Azzopardi, B., Hills, J., 2003. In: Bertola, V. (Ed.), Modelling and Experimentation in Two-phase Flow. Springer, Wien, NY.

Baum, E.B., Haussler, D., 1989. What size net gives valid generalization? Neural Comput. 1, 151–160.

Bezdek, J., 1981. Pattern Recognition with Fuzzy Objective Function Algorithms. Plenum Press, New York.

Bishop, C., 1995. Neural Networks for Pattern Recognition. Clarendon Press, Oxford.

Bowman, A.W., Azzalini, A., 1997. Applied Smoothing Techniques for Data Analysis. Oxford University Press.

Bromberg, M., Chang, T.S., 1992. One dimensional global optimization using linear lower bounds. In: Floudas, C.A., Pardalos, P.M. (Eds.), Recent Advances in Global Optimization. Princeton University Press, pp. 200–220.

Broomhead, D.S., Lowe, D., 1988. Multivariable functional interpolation and adaptive networks. Complex Syst. 2, 321–355.

Cai, S., Toral, H., Qiu, J., Archer, J.A., 1994. Neural network based objective flow regime identification in air–water two phase flow. Can. J. Chem. Eng. 72 (3), 440–445.

Cai, Y., Wambsganss, M.W., Jendrzejczyk, J.A., 1996. Application of chaos theory in identification of two-phase flow patterns and transitions in a small, horizontal, rectangular channel. J. Fluid. Eng. 118, 383–390.

Costigan, G., Whalley, P.B., 1997. Slug flow regime identification from dynamic void fraction measurements in vertical air–water flows. Int. J. Multiphase Flow 23, 263–282.

Das, R.K., Pattanayak, S., 1993. Electrical impedance method for flow regime identification in vertical upward gas–liquid two-phase flow. Measure. Sci. Technol. 4, 1457–1463.

Davies, R.M., Taylor, G.I., 1950. The mechanics of large gas bubbles rising through liquid in tubes. Proc. Roy. Soc. London, A 200, 375–390.

Ding, H., Huang, Z., Song, Z., Yan, Y., 2007. Hilbert–Huang transform based signal analysis for the characterization of gas–liquid two-phase flow. Flow Measure. Instrum. 18, 37–46.

Drahos, J., Cermak, J., 1989. Diagnostics of gas–liquid flow patterns in chemical-engineering systems. Chem. Eng. Process 26, 147–164.

Elperin, T., Klochko, M., 2002. Flow regime identification in a two-phase flow using wavelet transform. Exp. Fluids 32, 674–682.

Fagundes Netto, J.R., Fabre, J., Pereson, L., 1999. Shape of long bubbles in horizontal flow. Int. J. Multiphase Flow 25, 1129–1160.

Friedman, N., Geiger, D., Goldszmidt, M., 1997. Bayesian network classifiers. Mach. Learn. 29, 131–163.

Giarratano, J.C., Riley, G., 1994. Expert Systems: Principles and Programming. PWS Publishing Co., Boston.

Groot, C.D., Würtz, D., 1994. Plain backpropagation and advanced optimization algorithms: a comparative study. Neurocomput. NEUCOM 291, 153–161.

Hayes-Roth, F., Waterman, D.A., Lenat, D.B., 1983. Building Expert Systems, fourth ed. Addison-Wesley.

He, Q., 1998. Studying on progress of fuzzy clustering analysis theory and its application. Fuzzy Syst. Math. 12, 89–94.

Hernandez, L., Juliá, J.E., Chiva, S., Paranjape, S., Ishii, M., 2006. Fast classification of two-phase flow regimes based on conductivity signals and artificial neural networks. Measure. Sci. Technol. 17, 1511–1521.

Hervieu, E., Seleghim Jr., P., 1998. An objective indicator for two-phase flow pattern transition. Nucl. Eng. Des. 184, 421–435.

Hewiit, G.F., Hall Taylor, N.S., 1970. Annular Two-phase Flow. Pergamon Press Ltd., Oxford.

Hewiit, G.F., Jayanti, S., 1993. To churn or not to churn. Int. J. Multiphase Flow 19, 527–529.

Huang, S., Zhang, X., Wang, D., Lin, Z., 2008. Equivalent water layer height (EWLH) measurement by a single-wire capacitance probe in gas–liquid flows. Int. J. Multiphase Flow 34, 809–818.

Jana, A.K., Das, G., Das, P.K., 2006. Flow regime identification of two-phase liquid–liquid upflow through vertical pipe. Chem. Eng. Sci. 61, 1500–1515.

Jayanti, S., Hewitt, G.F., 1992. Prediction of the slug-to-churn flow transition in vertical two-phase flow. Int. J. Multiphase Flow 18, 847–860.

Jolliffe, I.T., 1986. Principal Components Analysis. Springer, NY.

Jones, O.C., Zuber, N., 1975. The interrelation between void fraction fluctuations and flow patterns in two-phase flow. Int. J. Multiphase Flow 2, 273–306.

Juliá, J.E., Liu, Y., Paranjape, S., Ishii, M., 2008. Upward vertical two-phase flow local flow regime identification using neural network techniques. Nucl. Eng. Des. 238, 156–169.

Kohonen, T., 1982. Self-organized formation of topologically correct feature maps. Biol. Cybern. 43, 59–69.

Kohonen, T., 2001. In: Self-organizing Maps, third ed.. Springer Series in Information Sciences, vol. 30 Springer, New York.

Lee, J.Y., Ishii, M., Kim, N.S., 2008. Instantaneous and objective flow regime identification method for the vertical upward and downward co-current two-phase flow. Int. J. Heat Mass Transfer 51, 3442–3459.

Lowe, D.C., Rezkallah, K.S., 1999. Flow regime identification in microgravity two-phase flows using void fraction signals. Int. J. Multiphase Flow 25, 433–457.

MacQueen, J., 1967. Some methods for classification and analysis of multivariate observation. Proc. of 5th Berkeley Symposium on Mathematical Statistics and Probability, vol. 1. Univ. of California Press, pp. 281–297.

Mahvash, A., Ross, A., 2008. Two-phase flow pattern identification using continuous hidden Markov model. Int. J. Multiphase Flow 34 (3), 303–311.

Matsui, G., 1984. Identification of flow regimes in vertical gas liquid two-phase flows using differential pressure fluctuation. Int. J. Multiphase Flow 10, 711–720.

Matsui, G., 1986. Automatic identification of flow regimes in vertical two-phase flows using differential pressure fluctuations. Nucl. Eng. Des. 95, 221–231.

Mi, Y., Ishii, M., Tsoukalas, L.H., 1998. Vertical two-phase flow identification using advanced instrumentation and neural networks. Nucl. Eng. Des. 184, 409–420.

Mishima, M., Ishii, M., 1984. Flow regime transition criteria for upward two-phase flow in vertical tubes. Int. J. Heat Mass Transfer 27, 723–737.

Omebere-Iyari, N.K., Azzopardi, B.L., Lucas, D., Beyer, M., Prasser, H.-M., 2008. The characteristics of gas/liquid flow in large risers at high pressures. Int. J. Multiphase Flow 34, 461–476.

Ruder, Z., Hanratty, T.J., 1990. A definition of gas–liquid plug flow in horizontal pipes. Int. J. Multiphase Flow 16, 233–242.

Rumelhart, D.E., Hinton, G., Williams, R., 1986. Learning internal representation by error propagation. Parallel Distributed Processing, vol. 1. MIT Press, Cambridge, MA, pp. 318–362.

Samaras, V.C., Margaris, D.P., 2005. Two-phase flow regime maps for air-lift pump vertical upward gas–liquid flow. Int. J. Multiphase Flow 31, 757–766.

Song, C.H., Chung, M.K., No, H.C., 1998. Measurements of void fraction by an improved multi-channel conductance void meter. Nucl. Eng. Des. 184, 269–285.

Specht, D., 1990. Probabilistic Neural Networks. Neural Networks 1, 109–118.

Taitel, Y., Barnea, D., Dukler, A.E., 1980. Modeling flow pattern transitions for steady upward gas–liquid flow in vertical tubes. AIChE J. 26, 345–354.

Tambouratzis, T., Pázsit, I., 2009. Non-invasive on-line two-phase flow regime identification employing artificial neural networks. Ann. Nucl. Energy 36, 464–469.

Tan, C., Dong, F., Wu, M., 2007. Identification of gas/liquid two-phase flow regime through ERT-based measurement and feature extraction. Flow Measure. Instrum. 18, 255–261.

Tutu, N.K., 1982. Pressure fluctuation and flow pattern recognition in vertical two-phase gas–liquid flows. Int. J. Multiphase Flow 8, 443–447.

Wada, S., Kikura, H., Aritomi, M., 2006. Pattern recognition and signal processing of ultrasonic echo signal on two-phase flow. Flow Measure. Instrum. 17, 207–224.

Wang, Y.W., Pei, B.S., Lin, W.K., 1990. Verification of using a single void fraction sensor to identify two-phase flow patterns. Nucl. Technol. 95, 87–94.

Waterman, D., 1986. A Guide to Expert Systems. Addison-Wesley.

Wu, H., Zhou, F., Wu, Y., 2001. Intelligent identification system of flow regime of oil–gas–water multiphase flow. Int. J. Multiphase Flow 27, 459–475.

Xie, T., Ghiasasiaan, S.M., Karrila, S., 2003. Flow regime identification in gas–liquid–pulp fiber flow based on pressure fluctuations using ANN. Ind. Eng. Chem. Res. 42, 7014–7024.

Xie, T., Ghiasiaan, S.M., Karrila, S., 2004. Artificial neural network approach for flow regime classification in gas–liquid–fiber flows based on frequency domain analysis of pressure signals. Chem. Eng. Sci. 59, 2241–2251.

Yan, H., Liu, Y.H., Liu, C.T., 2004. Identification of flow regimes using back-propagation networks trained on simulated data based on a capacitance tomography sensor. Measure. Sci. Technol. 15, 432–436.